Isotope and Pressure Dependence of Liquid–Liquid Equilibria in Polymer Solutions. 5. Measurements of Solute and Solvent Isotope Effects in Polystyrene–Acetone and Polystyrene–Methylcyclopentane. 6. A Continuous Polydisperse Thermodynamic Interpretation of Demixing Measurements in Polystyrene–Acetone and Polystyrene–Methylcyclopentane Solutions

Marek Luszczyk,† Luis P. N. Rebelo,‡ and W. Alexander Van Hook*

Chemistry Department, University of Tennessee, Knoxville, Tennessee 37996-1600

Received April 29, 1994; Revised Manuscript Received August 22, 1994®

ABSTRACT: Cloud and spinodal loci have been obtained as functions of pressure (P), temperature (T), polymer molecular weight (MW), polymer fraction, and H/D substitution on solute (z_D) or solvent (y_D), for acetone–polystyrene and methylcyclopentane–polystyrene solutions. A light scattering technique was employed. The isotope effects and their pressure dependences are large. An increase in pressure, an increase in H/D ratio in the solvent (or decrease in the polymer H/D ratio), or a decrease in polymer molecular weight increases the region of miscibility. The solutions show both upper and lower branches, which, for acetone, join at a hypercritical point. The cloud point diagrams are highly distorted in the hypercritical region but smooth as one moves away by appropriately varying pressure, H/D ratio, or solute molecular weight. In the vicinity of the multiple critical point, hypercritical distortion for polystyrene/$(CH_3)_2CO$ solutions causes a highly unusual homogeneous one-phase "hole" in the (T,W_{ps}) cloud point diagram. This "extra" one-phase region appears close to the hypercritical point, and just inside the two-phase region which forms immediately after the system collapses into the "hourglass" configuration. The effect is not seen in $(CD_3)_2CO$ or mixed $(CH_3)_2CO/(CD_3)_2CO$ solutions, but those solutions also show marked distortion in the (T,W_{ps}) plane. H/D substitutions (on either polymer or solvent) cause large differences in cloud point and spinodal temperatures, especially in the vicinity of the hypercritical point. Isotope shifts as large as 40 K were observed on the cloud points of the polystyrene/acetone system. A mean-field formalism to interpret cloud point and spinodal data on liquid–liquid demixing of polymer–solvent solutions exhibiting both upper and lower consolute branches and hypercritical points is developed. The dependence of the phase equilibria on pressure, temperature, segment number, polydispersity, and H/D substitution of either or both solvent and polymer are explicitly considered. Calculations of cloud and shadow curves are reported. The method is based on a Flory–Huggins type continuous thermodynamic representation of free energies in polydisperse polymer solutions due to Ratzsch and co-workers. The computer algorithm PHASEEQ^r written in QUICKBASIC^r has been coded for the case of Schulz–Flory segment distribution functions. Calculations interpreting demixing data for polystyrene/acetone and polystyrene/methylcyclopentane solutions over wide ranges of pressure, concentration, molecular weight, and H/D substitution are reported. The isotope effects, which are large, are discussed using Bigeleisen–Van Hook–Wolfsberg condensed phase isotope effect theory. Along the critical line multidimensional classical or nonclassical scaling equations permit economical representation of the data. The scaling approach is developed and compared with the mean-field based interpretation.

1. Introduction

Polymer miscibility is an important topic of research because the physical properties of polymer blends depend not only on the molecular parameters of each component but also, and sometimes very sensitively, on phase equilibria in the mixture. Szydlowski and Van Hook[1] have commented that investigations of isotope effects (IE's) on physical properties of condensed phase molecules,[2–4] including IE's on phase equilibria, can contribute significantly to our knowledge of the nature of such solutions, including understanding at the molecular level. Similarly, the importance of pressure effects on phase equilibria are well established,[5,6] and that importance has recently been reemphasized,[7,8] even though most cloud point (CP) or coexistence measurements to be found in the literature have been measured at the vapor pressure of the sample or at atmospheric pressure. Thus it seems clear that the determination of accurate pressure and isotope dependences for CP's in addition to their dependence on temperature, concentration, molecular weight, polydispersity, *etc.*, can materially aid fundamental understanding of such solutions.

The conditions defining phase equilibria and phase equilibria IE's are sensitive functions of the potential energy surface (PES) which describes the solution in terms of atomic and molecular motion. PES is closely related to the thermodynamic equation of state. IE measurements are useful because PES is independent of isotope substitution; therefore combining IE measurements with other kinds of thermodynamic information, and with spectroscopic and other data, can lead to refinement of the models used to describe solutions.

A thorough knowledge of IE's in polymer solutions is required for proper interpretation of neutron scattering results. H/D mixtures are widely employed in scatter-

* To whom correspondence should be addressed.
† On leave at the University of Tennessee 1992–94. Permanent address: Institute of Physical Chemistry, Warsaw.
‡ On leave at the University of Tennessee 1990–91. Permanent address: Department of Chemistry, New University of Lisbon, 2825 Monte da Caparica, Lisbon, Portugal.
® Abstract published in *Advance ACS Abstracts,* January 15, 1995.

0024-9297/95/2228-0745$09.00/0

ing experiments in order to enhance sensitivity and contrast. Most authors have elected a tracer model for interpretation but this ignores excess thermodynamic properties of mixtures of isotopomers and other complications. Van Hook and co-authors[1,4] have reviewed the relevant literature. This includes a number of reports of IE's on Θ temperatures and other thermodynamic properties, as well as papers which consider the effects of nonideality in H/D isotopomer mixtures.[9-12]

We have reported the construction and preliminary use of an apparatus to detect phase separation in polymer–solvent mixtures at elevated pressures[1,13-15] and have chosen to study systems with upper and lower consolute branches. Patterson and co-workers,[16,17] Saeki *et al.*,[18] and Hosokawa, Nakata, and Dobashi[19] have previously reported on the pressure dependences of phase transitions for polystyrene solutions (but for protiated samples only). In the present paper we report extensive data on the pressure, H/D, and molecular weight dependence of UCS and LCS type liquid–liquid precipitation cloud and spinodal loci in acetone–polystyrene ($(CH_3)_2CO$/PS(h), $(CD_3)_2CO$/PS(h), $(CH_3)_2CO$/PS(d), and $(CD_3)_2CO$/PS(d)) and methylcyclopentane–polystyrene ($C_5H_9CH_3$/PS(h), $C_5D_9CD_3$/PS(h), $C_5H_9CH_3$/PS(d), and $C_5D_9CD_3$/PS(d)) solutions. For acetone solutions we have paid particular attention to the hypercritical region, where the UCS and LCS branches merge, and the system undergoes a transition to the "hourglass" configuration.

The objective of the second part of the paper is to interpret polymer–solvent demixing data taking account of polydispersity in order to properly rationalize fractionations in ψ, r, ϱ_m, y_D, and z_D. Throughout we denote the segment fraction polymer by ψ, the number of segments by r, and the polydispersity index by $\varrho_m = M_w/M_n$, where M_w is the weight average molecular weight and M_n the number average molecular weight. Also the weight fraction polymer will be denoted W_{ps}, the volume fraction polymer ϕ, and isotope concentrations on the solvent and solute will be labeled $y_D = (n_D/(n_D + n_H))_{solvent}$ and $z_D = (n_D/(n_D + n_H))_{solute}$, n_i is the number of atoms of type i.

In the material which follows we report calculations of CP diagrams based on a mean-field continuous thermodynamic representation of free energies in polydisperse polymer solutions developed by Ratzsch and co-workers.[20] That complete, we will briefly discuss multidimensional scaling descriptions as an economic method to represent the large amounts of data expected to result from the present program and then turn attention to interpretation of the isotope effect (IE) data. Jancso, Rebelo, and Van Hook[3,4] have reviewed the thermodynamics of IE's and isotopomer mixtures and have summarized reasons for the usefulness of such data.

2. Experimental Section

2a. Equipment. The data reported below were obtained with equipment described by Szydlowski, Rebelo, and Van Hook.[13,14] The method takes advantage of the intensity changes in transmitted and forward scattered light which occur when a polymer/solvent mixture contained in a capillary high-pressure cell undergoes a phase transition induced by changing the cell temperature at a given pressure, by changing its pressure at a given temperature, or by some combination of changes. Pressure (±0.001 MPa, $0 \le P/\text{MPa} \le 7$) and temperature (±0.001 K, $235 \le T/\text{K} \le 573$) are under computer control, and both pressure/time and/or temperature/time profiles are programmable. In the present experiments the top-cap of the capillary cell was fitted with an HPLC valve (Valco HPLC-C6U) which can place either one of two dilution syringes into contact with the sample chamber. The improvement permits measurements to be made at several different concentrations with a single polymer charge.

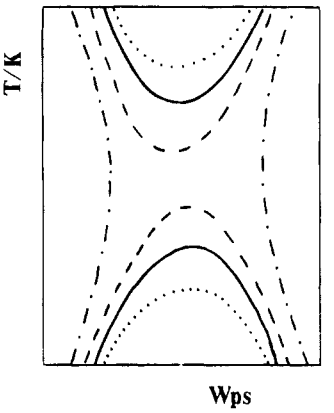

Figure 1. Schematic showing the effect of molecular weight and/or pressure, and/or H/D substitution on phase diagrams with both UCST and LCST branches. By lowering pressure, increasing solvent D/H ratio, or raising solute MW, one decreases miscibility (see the succession "dotted → solid → dashed" lines). At low enough pressure, high enough molecular weight, *etc.*, the two branches join into the "hourglass" configuration (heavier dash-dot lines to left and right). Were the system strictly binary, the point of collapse would be a true hypercritical point. (Compare with Figure 10.)

Cloud points are detected optically. Light from a 5 MW He–Ne laser is transmitted through an optical cable to the cell. The transmitted exit light at 180° nominal geometry enters the central portion of a bifurcated optical cable, while low angle scattered light ($2 \le 2\theta/\text{deg} \le 4$) falls on the outer portion. The scheme of the experiment may be described using the idealized diagram, Figure 1, which schematizes the effects of pressure, isotope substitution, and MW, on solutions with both UCS and LCS branches using the monodisperse approximation. We begin with a homogeneous solution in the near hypercritical region. By lowering the pressure, raising the solute molecular weight, deuterating the solvent (or protiating the polymer solute), one moves in the direction of decreasing the region of miscibility (as shown by the sequence of lines: dotted → solid → dashed). At low enough pressure, or high enough molecular weight, the two branches join, and the system collapses into the "hourglass" configuration (dash-dot line). If the solution were a true binary mixture (it is not, because of the distribution in solute molecular weights), that point of collapse would be a true hypercritical point. In the present experiments, the system, initially in the homogeneous one-phase central portion of the diagram is displaced into the two-phase region, while transmitted and scattered light, temperature, and pressure are monitored. This may be accomplished by varying temperature and/or pressure, but it is rather more convenient, and more efficient, to vary pressure (isothermally) than temperature (isobarically). The solutions were not stirred or circulated during the measurements to avoid shear effects.[21]

Examples of light scattering profiles for liquid–liquid transitions have been shown previously.[1,14] At the beginning of an experiment the solution is homogeneous and at an appropriate temperature and (elevated) pressure. Pressure (temperature) is changed according to a preselected program and precipitation induced. The raw data show a decrease in transmitted and an increase in scattered intensity as pressure falls. Scattered intensity is corrected for stray reflection and multiple scattering using the attenuation of the transmitted beam to define a correction factor. Following Kiepen and Borchard[22] the cloud-point (CP) locus, $(T,P)_{cp}$, is equated to that point on the $1/I_{sc,corr}$ *vs* P (or T) curve where the slope changes abruptly, and the operational spinodal (SP) to the $1/I_{sc,corr} = 0$ intercept.[22,23] We adhere to this operational definition throughout the present paper. In the mean-field

Table 1. Characteristics of Polystyrene-*h* and Polystyrene-*d* Samples[a]

code	polymer	M_w*	M_w*/M_n**	source[b]
A	PS(h_8)-4.0	4136	≤1.06	PC-30525
B	Ps(h_8)-7.5	8000	≤1.09	PC-80314
C	PS(h_8)-11.6	11687	1.03	PL-20130/3
D	PS(h_8)-13.5	13502	≤1.06	PC-30420
E	PS(h_8)-22.0	22091	1.03	PL-20131/2
F	PS(h_8)-25.0	25000	≤1.06	PC-30811
G	PS(h_8)-106.0	106280	≤1.06	PC-61126
H	PS(d_8)-10.5[c]	10512	1.02	PL-20629/1
I	PS(d_8)-27.0[c]	26890	1.06	PL-20632/1

[a] Weight average molecular weight (M_w*) data supplied by manufacturer using gel permeation chromatography (*); number average (M_w**), by size exclusion chromatography (**). [b] PL = Polymer Laboratories, Amherst, MA; PC = Pressure Chemical, Pittsburgh, PA. Lot numbers are shown. [c] $z_D = n_{PS(d)}/(n_{PS(d)} + n_{PS(h)}) > 0.98$.

approximation SP corresponds to a point of inflection on the free energy surface. However, blind application of mean-field theory in the critical region is inappropriate, and for this and other reasons de Gennes[24] has questioned whether SP has a precise experimental meaning. Even so, the present definition of the SP isopleth as the $(T,P)_{sp}$ locus where $(1/I_{corr,sc}) \rightarrow 0$ is operationally unambiguous. Using Debye plots[22,23] we have found that CP temperatures (or the equivalent pressures) can be assigned reproducibly with a precision of about 0.01 K (or equivalent, ≈0.01 MPa), but the operational SP temperatures (pressures) are somewhat less precise (uncertainties are in the range ±0.01 to ±0.1 K (or the equivalent pressure uncertainty), sometimes worse). Sample-to-sample reproducibility is worse.

The laborious procedure for data workup described above is not always necessary. For strong scatterers the marked kink in $1/I_{sc,corr}$ plots manifests an equally strong kink in the uncorrected (I_{sc},P) or (I_{sc},T) plots. In that case CP loci can be picked from the computer-screen plots of the raw data with little or no loss in accuracy. On the other hand SP data require the complete analysis. Unless otherwise noted, data reported in this paper have been obtained using the Debye procedure.

2b. Materials. H and D substituted polystyrenes of well-defined molecular weight and molecular weight distribution were obtained from Polymer Laboratories or Chemical Pressure Co. and are described in Table 1. The samples were vacuum dried (≈60 °C) and solutions made up gravimetrically. Rollins, Scrivens, Taylor, and Major[25] have reported mass spectrometer analyses of molecular weight distributions for some of the lower MW Polymer Laboratories samples, these measurements nicely complement the $\varrho_m = M_w/M_n$ data supplied by the manufacturer.

Acetone and deuterioacetone were purified as earlier described.[1] Deuteriomethylcyclopentane (MCP-*d*) was prepared from D_2O and C_6D_6 by Yijun[26] in a two-step process. Electrolytically produced D_2 was bubbled through C_6D_6 at 33 °C and the mixture passed over a charcoal supported Pt catalyst at atmospheric pressure and 200 °C to yield C_6D_{12}. In the second step C_6D_{12} was refluxed at 70 °C over an $AlCl_3$ catalyst moistened with D_2O, the system reaching equilibrium at about 22% MCP-*d* at 5 h, after which MCP-*d* was slowly stripped from the top of the ≈10 plate flux column as reaction continued. The crude product was treated with concentrated H_2SO_4 to remove C_6D_6, washed with water, dried over $CaCl_2$ and distilled in a spinning band column. The fractional deuteration determined by NMR was 0.943.

3. Results

CP and SP temperatures and pressures are reported as a function of concentration and solvent H/D ratio for PS-*h*/ and PS-*d*/acetone solutions in Table 2SUPP (SUPPlemental materials), and for PS-*h*- and PSd/methylcyclopentane solutions in Table 4SUPP. For acetone-*h*/acetone-*d* solutions Table 2SUPP reports information on 65 PS solutions, 250 < *T*/K < 375, 0 < y_D < 1, 0 < *P*/MPa < 5, 0.1 < W_{ps} < 0.3, 7.5 < MW/kg·mol^{-1} < 22.0, and $z_D = 0$ or 1. (y_D is the atom fraction D of solvent (H + D), z_D is the atom fraction D of polymer (H + D)). Table 4SUPP gives similar information for PS/MCP-*h* and PS/MCP-*d* solutions over a broader range of MW. Tables 3SUPP and 5SUPP report least squares fits of the isopleth data, (P_{cp} *vs* T_{cp}) and (P_{sp} *vs* T_{sp}), using one or another of eqs 1–4.

$$T_{cp} = A_1 + B_1P \quad (1)$$

$$T_{sp} = A_2 + B_2P \quad (2)$$

$$P_{cp} = D_3 + E_3T + F_3T^2 + G_3T^3 \quad (3)$$

$$P_{sp} = D_4 + E_4T + F_4T^2 + G_4T^3 \quad (4)$$

For these measurements precipitation was isothermally induced by decreasing pressure at an appropriate rate. After sufficient scattering data (I_{sc} *vs* $P)_T$ were collected, the sample was repressurized, stirred, and warmed to a new temperature and the procedure repeated. Data for 5–10 $(T,P)_{transition}$ sets sufficed to determine a single isopleth at each concentration (W_{ps}), after which the sample was diluted or replaced. Present procedures allow measurements at two or three concentrations each day.

Each individual $(T,P)_{cp}$, $(T,P)_{sp}$ data pair in a given W_{ps} data set consists of approximately 20–100 (T,P,I_{trans},I_{sc}) scattering measurements collected at 8 s intervals. In the usual case *P*, the independent variable, is changed a total of several MPa in equally spaced steps of several hundreths MPa. SP intercepts and CP kinks are reported in Tables 2SUPP–5SUPP. We adhere to the operational definitions for CP and SP given above. Figure 2 shows isopleths for a set of solutions with an hypercritical point (Figure 2c) and compares that data with isopleths far from $(T,P)_{hcp}$ (Figures 2a and 2b). The precision is typically $\delta P \approx \pm 0.01$ MPa and $\delta T \approx \pm 0.01$ K. Sample-to-sample variations are larger.

The data in this paper report CP and SP curves. CP and SP are functions of weight fraction, pressure, molecular weight, and molecular weight distribution, $T_{cp} = T_{cp}(W_{ps},P,M_w,\varrho_m)$, and only for solutions of monodisperse polymers, $\varrho_m = 1$, do CP and coexistence curves coincide. For the monodisperse case we prefer to employ the term binodal (BIN), obviously referring to the fact that the MW distribution is precisely binodal with just one solute and one solvent MW. Molecular weight dispersions, $\varrho_m = M_w/M_n$, for the polymers employed in this work are reported in Table 1 ($1.02 \leq \varrho_m \leq 1.09$), all except one lie at or below $\varrho_m = 1.06$. The samples are among the narrowest commercially available and for such narrow MW dispersions many previous authors, some,[16–19] but not all referenced in this paper, have elected the simplification of equating CP and BIN.

It is commonly stated that the critical concentration lies at a point of tangency of the SP and CP curves and most of the present data fit that criterion reasonably well (within a few tenths K or so). It is well established that maxima in the CP and SP curves need not coincide, and in fact usually do not coincide.[27,28] The pressure dependences of the operational critical temperatures can be obtained from Tables 2SUPP–5SUPP using an interpolation procedure. (In the hypercritical region, and particularly toward the low concentration side of the maximum, SP is difficult to define experimentally, primarily because of large multiple scattering correc-

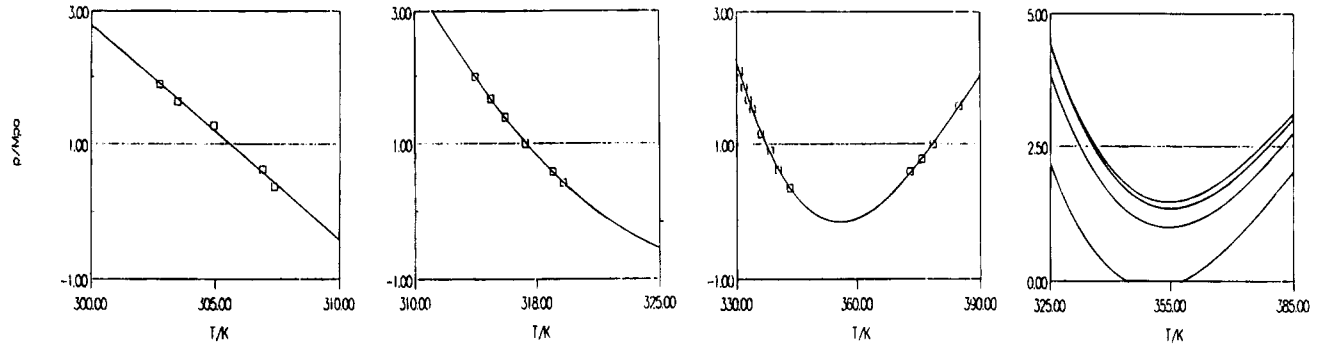

Figure 2. (a–c, left to right) $(T,P)_{cp}$ isopleths at various concentrations for solutions of PS(h) = 13.5 kg·mol^{-1} in acetone. Reading from left to right y_D = 0.483, 0.719, 0.952. (d, far right) A set of isopleths for PS(h) = 17.8 kg·mol^{-1} + (0.5acetone-h + 0.5acetone-d). From top to bottom W_{ps} = 0.209, 0.236, 0.245, 0.265.

tions. Near the hypercritical point the diagrams become highly distorted because of the infinities in $(\partial T/\partial P)_{hcp}$, $(\partial T/\partial MW^{-1})_{hcp}$, *etc.* Some consequences are discussed in the sections which follow.)

The pressure dependence of W_{ps}(cr) is small and we were unable to determine it to better than a crude estimate. Since the experiments establish $(\partial W_{ps}(cr)/\partial P)$ to be small over the range of pressure of interest to us (0–4 MPa, or so), we have not considered this coefficient any further.

4. Discussion

A large quantity of data has been summarized in the supplementary materials. CP and SP temperatures, T_{cp} or T_{sp}, are functions of at least six variables; $T_{cp\ or\ sp} = T(MW,\varrho_m,W_{ps},y_D,z_D,P,...)$.

4.1. Acetone–Polystyrene Demixing in the Hypercritical Region. 4.1a. (T,W_{ps}) Projections at Constant MW_{hcp}, $\varrho_{MW}y_D$, z_D, and P. To study phase transitions in the hypercritical region we selected PS samples with MW and ϱ_m to give a hypercritical transition at convenient pressure. Figure 3 demonstrates the high sensitivity of hypercritical demixing to pressure (follow sequences left to right) and isotopic substitution (sequences top to bottom). To begin, notice the large solvent isotope effect on the hypercritical molecular weight MW_{hcp}. Thus in $(CH_3)_2CO$ (y_D = 0, z_D = 0), the hypercritical conditions at $P \approx$ 0.43 MPa are (T_{hcp}, MW_{hcp}) = (346.33 K, 22.0 kg·mol^{-1}). Hypercritical conditions shift dramatically on solvent deuteration. For $(CD_3)_2CO$ (y_D = 1, z_D = 0), (T_{hcp}, MW_{hcp}) = (358.83 K, 13.5 kg·mol^{-1}) at P = 0.29 MPa. For the mixed solvent–mixed solute system (y_D = 0.5, z_D = 0, MW_{hcp} = 17.8 kg·mol^{-1} [but with a bimodal MW distribution of 0.5 weight fraction (wt fr) PS(h) = 13.5 kg·mol^{-1} and 0.5 wt fr PS(h) = 22.0 kg·mol^{-1}]), the pressure dependence is shown at the bottom where (T_{hcp}, P_{hcp}) = (354.52 K, 1.48 MPa). It is interesting to compare the solvent H/D dependence with that for polymer deuteration. For solutions deuterated on both polymer and solvent, $(CD_3)_2CO$/PS-d (y_D = 1, z_D = 1), (T_{hcp}, MW_{hcp}) = (351.23 K, 27.2 kg·mol^{-1}) at P = 2.62 MPa (these measurements are not shown in Figure 3). Both CP and SP are sensitive to deuteration on the polymer, but the sign of the IE is opposite to that for solvent deuteration.

The data illustrated in Figure 3 establish remarkably large solute and solvent IE's on MW_{hcp} for PS/acetone solutions. Typically, perprotio/perdeuterio IE's, for example vapor pressure IE's, are on the order of a few percent or so at room temperature and above,[3] but the present solvent IE's on MW_{hcp} are 1 order of magnitude larger. Thus it becomes important to establish whether the effects are intrinsically large or if there is some unusual critical amplification. In reporting hypercritical conditions, we have consistently chosen the point at which the upper and lower cloud point surfaces first touch at the critical concentration W_{ps}(cr). Because W_{ps}(cr) is usually not at the maximum of CPC, this merger of critical points is usually found after the point of first junction of the two surfaces. For example, in the top sequence in Figure 3 one sees that the CPC surfaces first intersect at about 0.46 MPa, in the middle sequence at 0.88 MPa. In both cases the first merger is at $W_{ps} < W_{ps}$(cr).

4.1b. (P_{hcp},W_{ps}) Projections at Constant MW_{hcp}, $\varrho_{MW}y_D$, z_D, and $\sim T_{hcp}$. An alternative projection of some of the data in Figure 3 is given in Figure 4. Here, holding MW, T, y_D, and z_D constant at their hypercritical values, we show cloud points in the (P_{hcp},W_{ps}) plane. Figures 4a, 4b, and 4c correspond to the upper, middle, and lower sequences in Figure 3, respectively. The cp diagrams in the (P_{hcp},W_{ps}) plane (Figure 4) reflect those in the (T,W_{ps}) plane (Figure 3) and illustrate self-consistency in the data net.

4.1c. Hypercritical Distortion. The shapes of the CPC $(T,W_{ps})_P$ diagrams in Figure 3 are interesting. In the immediate vicinity of the hypercritical point they are highly distorted from the idealized UCS/LCS shape of Figure 1. However, as one moves away from hypercritical conditions, the diagrams smooth. Figures 5a and 5b show UCS branches for PS(d_8) = 27 kg·mol^{-1} and PS(h) = 13.5 kg·mol^{-1} in $(CH_3)_2CO$ far from the hypercritical region. The curves display little or no distortion. The trend with solvent quality is analogous. MCP is a better solvent for PS than acetone, so much better that, although both UCS and LCS branches are observed, a hypercritical point is not accessible at finite MW. Figure 5c shows the (T,W_{ps}) diagram for PS(h) = 25 kg·mol^{-1} in MCP(h). Improved solvent quality is reflected in the formation of a more nearly symmetric diagram. Although solvent quality improves with pressure, the bimodal nature of the acetone–PS diagrams is clear even at conditions well removed from $(T,P)_{hcp}$, (see Figure 3 or Figure 5b). As pressure drops, the double maxima (and minima) for the UCS (and LCS) branches join. For PS(h) = 22 kg·mol^{-1} in acetone-h this leads to an unusual feature in the phase diagram which is discussed in the next section. The magnitude of $|(\partial T_c/\partial P)|$ is a sensitive probe of solvent quality and of the relative size of the miscibility window. Figure 6 shows plots of $|(\partial T_c/\partial P)|_{ucst}$ against polymer MW for several systems. The increase in $(\partial T_c/\partial P)$ as the hypercritical point is approached is apparent.

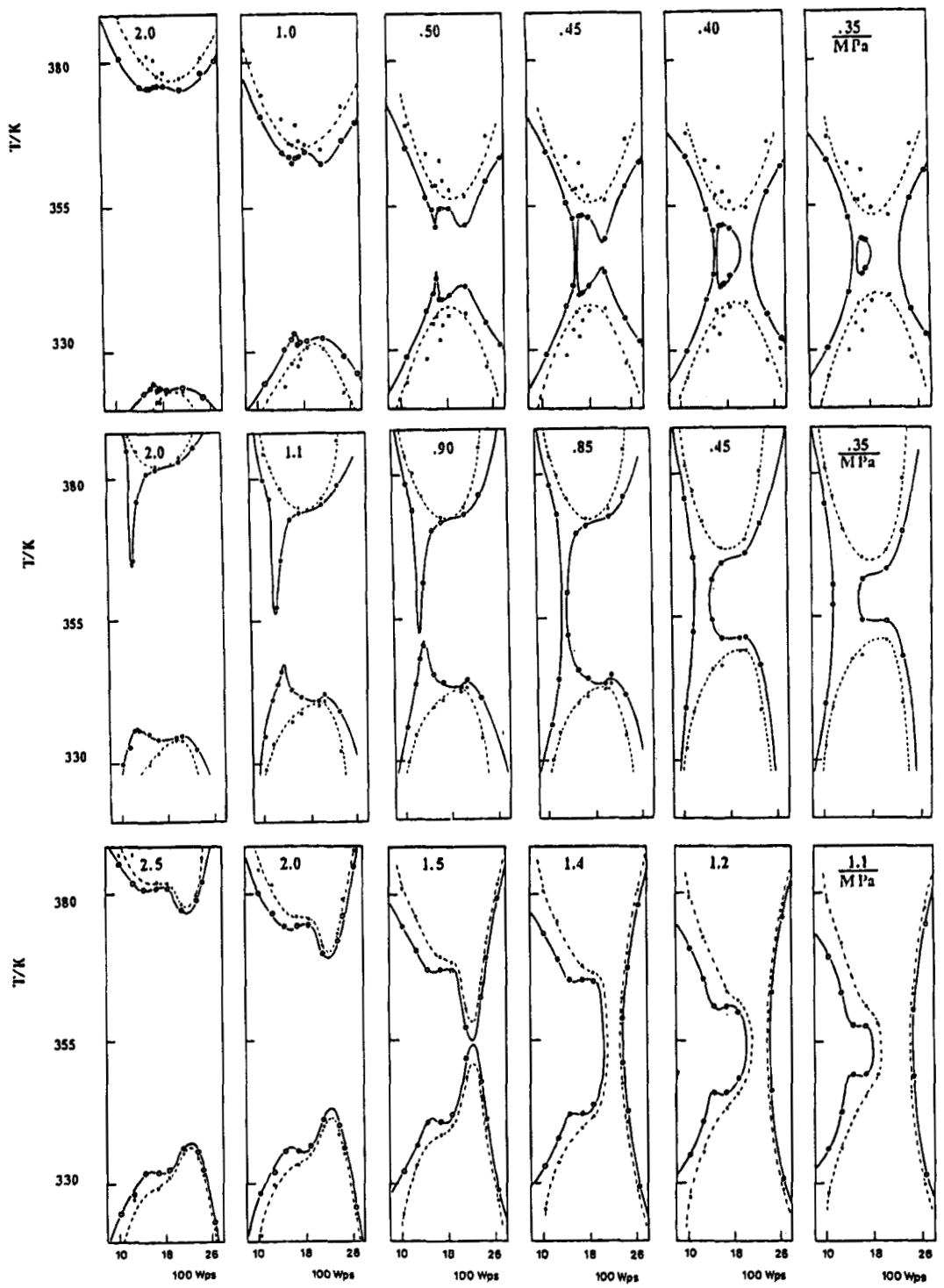

Figure 3. (T,W_{ps}) projections of phase separation in PS(h)/acetone solutions (z_D = 0) at some different pressures and ACh/ACd ratios. The effect of pressure is shown horizontally; that of H/D substitution on acetone, vertically. z_D is the D fraction in the solute; y_D, the D fraction in the solvent. The hypercritical molecular weight, MW_{hcp}, and the shape of both the UCS and LCS branches, especially the binodal (cloud point) branches are very sensitive to applied pressure as shown in the three left to right sequences. (a) upper sequence, PS = 22 kg·mol^{-1}/ACh (y_D = 0); (b) middle sequence, PS = 13.5 kg·mol^{-1}/ACd (y_D = 1); (c) lower sequence, PS = 17.8 kg·mol^{-1}/ACh$_{1/2}$d$_{1/2}$ (y_D = 0.5).

Continuing the discussion of solvent quality, recall that cyclohexane and methylcyclohexane are better solvents than MCP, their solutions are even further from hypercritical conditions. As expected, the (T,W_{ps}) plots for these solvents are smoother and more nearly ideal. In fact PS(h)/cyclohexane solutions, whose CPC's were studied by Schultz and Flory[29] more than 40 years ago, were used by Nakata and co-workers[30–32] in a classic series of coexistence measurements which established that generalized scaling with appropriate universal exponents applies to polymer solutions in the (T,W_{ps})$_P$ projection.

Returning to the discussion of distortion near T_{hcp}, recall that maxima in UCS, and minima in LCS cp curves, do not generally occur at W_{ps}(cr), *i.e* at the extrema of the SP curves. Most often (T,W_{ps})$_{cp}$ diagrams show only a shoulder or small local maximum (or minimum) at or near W_{ps}(cr); for a good example see the middle sequence in Figure 3. This type of behavior is well established, many examples have been dis-

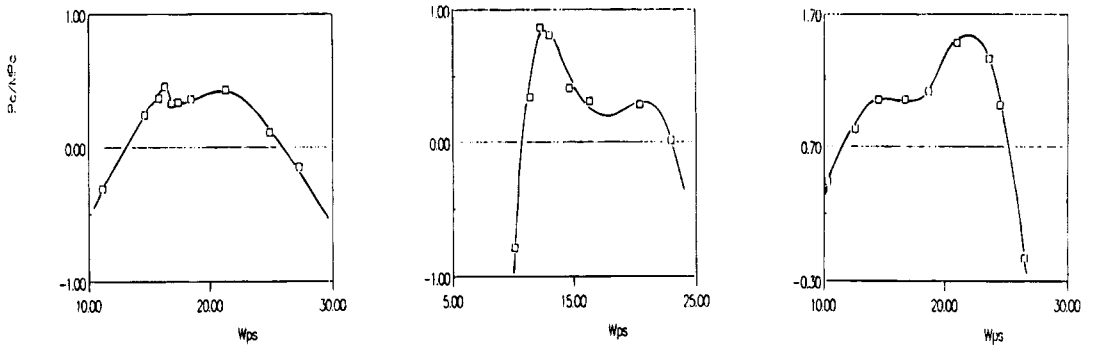

Figure 4. Cloud points in the (P_{hcp},W_{ps}) plane at hypercritical T, MW, y_D, and z_D as obtained from the data in Table 3. Figures 4a, 4b, and 4c (left to right) correspond to the upper, middle, and lower sequences in Figure 3. Notice the similarity in shape of the projections in Figures 3 and 4.

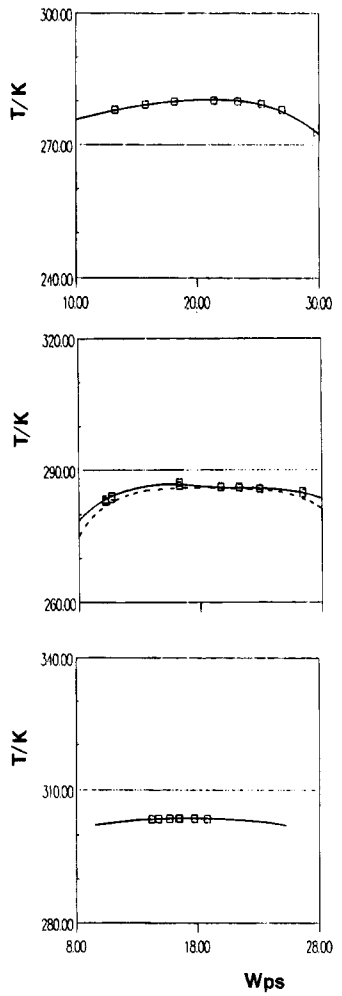

Figure 5. (T,W_{ps}) projections of UCS phase separation in two polystyrene/acetone-h solutions (z_D = 0 and z_D = 1, y_D = 0) and one polystyrene-h/MCP(h) solution. These systems are well removed from the hypercritical region and show little or no hypercritical distortion. (Compare with Figures 3 and 4). Top to bottom: PS(d) = 27 kg·mol^{-1}/ACh (y_D = 0); PS(h) = 13.5 kg·mol^{-1}/ACh (y_D = 0); (c) PS(h) = 25 kg·mol^{-1}/MCPh (y_D = 0).

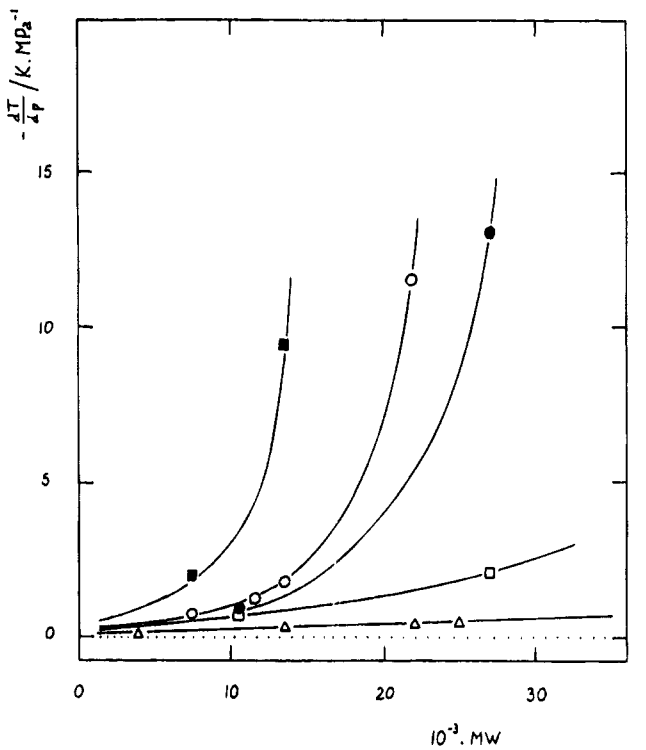

Figure 6. Some plots of (dT_{ucst}/dP) as a function of MW at varying distances from MW_{hcp} with $T \approx T_{hcp}$. ■ = PS(h) + AC(d). ○ = PS(h) + AC(h). ● = PS(d) + AC(d). □ = PS(d) + AC(h). △ = PS(h) + MCP(h).

cussed.[27,28] Most of the present solutions show W_{ps}(cr) > W_{ps}(cp(max)).

(i) The maximum in scattering intensity is found at the critical shoulder (spinodal maximum) where, for these solutions, transitions are sharp. As one moves away from the critical concentration, the optical quality of the transition degrades but not in any smooth fashion. Rather we have found that for concentrations between the W_{ps}(cp(max)) and W_{ps}(cr), and for concentrations beyond W_{ps}(cr) (*i.e* to the other side of the maximum from W_{ps}(cr), irrespective of whether W_{ps}(cp(max)) occurs to the right or to the left of W_{ps}(cr), the transitions remain sharp and well-defined. However at concentrations beyond W_{ps}(cp(max)), whether to the right or left of W_{ps}(cr), the optical quality (*i.e.* "sharpness") degrades rapidly as one goes beyond W_{ps}(cp(max)). We are not aware of any theoretical rationalization of this effect and think it worthy of further investigation.

(ii) At near-critical concentrations the cloud and spinodal (T,P,W_{ps}) loci, while close to each other, no longer coincide. The spinodal curve lies to the low-pressure side of cp and the difference between the two curves increases near T_{hcp} because of the hypercritical infinities. As an example consider ((PS(h) = 22.0 kg·mol^{-1} + acetone(h)), W_{ps} = 0.21), in the (T,P) plane, (Figure 7). The CP loci are labeled with the solid points; SP, with open points. The region inside the curve is homogeneous, line segments "AB_{cp}" and "CB_{cp}" show the pressure dependence of the CP LCS and UCS, respectively, and "AB_{sp}" and "CB_{sp}" similarly show the two

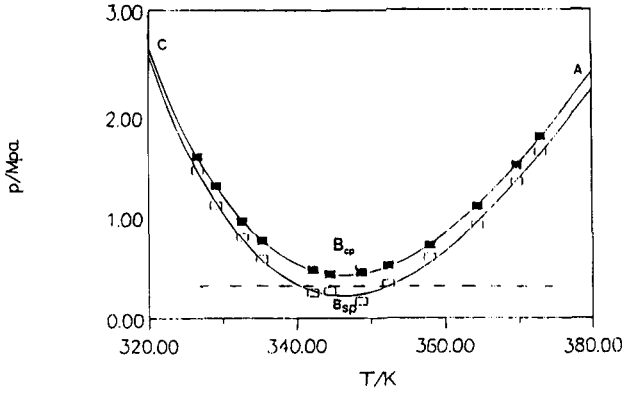

Figure 7. Cloud point and spinodal isopleths for ((PS(h) = 22 kg·mol^{-1} + AC(h)), W_{ps} = 0.21) in the near-hypercritical region. CP locus = solid points, SP locus = open points. The region inside the curve is one-phase homogeneous, line segments "AB_{cp}" and "CB_{cp}" show the pressure dependence of the CP ("binodal") LCS and UCS, respectively, and "AB_{sp}" and "CB_{sp}" similarly show the two branches SP. Left and right of the homogeneous region the system splits into two phases (UCS and LCS, respectively), and underneath the minimum it is in the two-phase hourglass configuration. Near T_{hcp} one can draw an isobar (dotted line) where SP remains in the UCS/LCS region, but Cp has dropped into the hourglass configuration. This will be the case whenever B_{sp} and B_{cp} do not coincide.

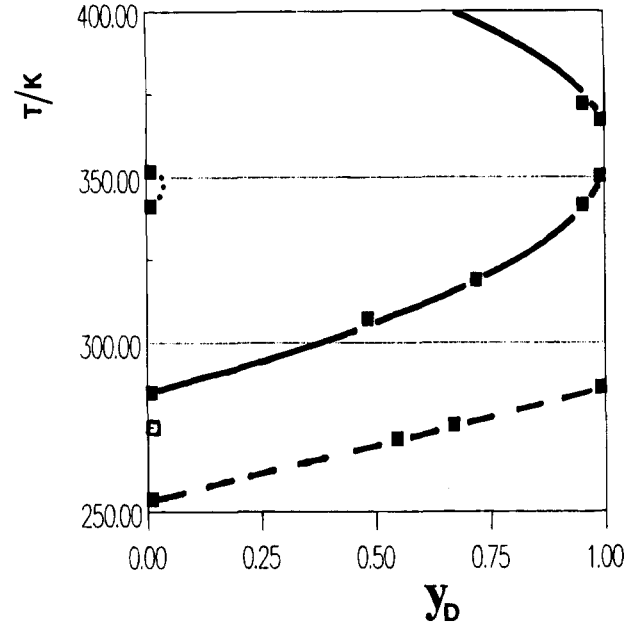

Figure 8. Solvent isotope effects on UCS (mostly) and LCS transition temperatures for some PS(h)/acetone solutions. Here $y_D = n((CD_3)_2CO)/(n((CD_3)_2CO) + n((CH_3)_2CO)$. ···■··· = PS($h$) = 22 kg·mol^{-1}; —■— = PS(h) = 13.5 kg·mol^{-1}; - - -■- - - = PS(h) = 7.5 kg·mol^{-1}; □ PS(h) = 11.6 kg·mol^{-1}.

branches of the SP curve. Left and right of the homgeneous region the system splits into two phases (UCS and LCS, respectively); underneath the minimum it is in the two-phase hourglass configuration. Near T_{hcp} one can draw an isobar (dotted line) where the spinodal remains in the UCS/LCS region, but CP has dropped into the hourglass configuration. This will be the case whenever B_{sp} and B_{cp} do not coincide. Evidence for this behavior is found in the data shown in various parts of Figure 3 and discussed in the next section. The isobars shown there demonstrate a considerable pressure range over which the CP surface has already made its transition to a distorted hourglass configuration, while the experimentally observed SP remain in the LCS/UCS conformation.

4.1d. An Unusual One Phase Region near T_{hcp}, P_{hcp}. The top sequence in Figure 3 shows CPC's in the hypercritical region for PS(h) = 22 kg·mol^{-1} in acetone ($y_D = z_D = 0$). For pressures just below P_{hcp} we have observed the formation of an isolated one-phase region in the middle of the developing "hourglass" configuration (*cf.* the two right-most diagrams at the top of Figure 3).[15] As pressure continues to fall, this "middle-one-phase" region contracts, and finally vanishes at a point, $p = p_{triple}$ = 0.33 MPa. Were the polymer is monodisperse, that point would be a triple point, but under the conditions in the diagram not a tricritical point.[15] It is, however, important to keep in mind that the molecular weight dispersions, $\varrho_m = M_w/M_n$, are different in each phase. We are not aware of any other report of a polymer–solvent system which displays a phase diagram analogous to the (PS(h) = 22 kg·mol^{-1} + $(CH_3)_2$-CO) diagram reported in Figure 3.

4.2. Solvent Isotope Dependence of the Critical Points. Figure 8 shows solvent IE data from Table 2SUPP plotted in the $(T,y_D)_{P=0.5}$ plane. Critical loci for four PS(h)/acetone solutions of different MWs are shown. The solvent IE on hypercritical molecular weight, MW_{hcp}, at this pressure (0.5 MPa) is established by comparing the hypercritical point for the curve at the extreme left (PS(h) = 22 kg·mol^{-1}, $y_D \approx 0.05$) with that for the curve at the right (with hypercritical point at PS(h) = 13.5 kg·mol^{-1}, $y_D \approx 1$, P = 0.5 MPa). Two phase regions lying below or above the envelopes exhibit UCS or LCS behavior. Those to the right of (T_{hcp},$y_{D,hcp}$) are in the "hourglass" configuration.

The bottom-most curve in Figure 8 reports the solvent IE for PS(h) = 7.5 kg·mol^{-1}/acetone solutions. $T_{cr,ucs}$ increases almost linearly with solvent deuteration. Deviations from linearity are less than 1%, even though the solvent isotope effect is large [$(\partial T_{cr,ucs}/\partial y_D)_{P=0.5}$ = 33.1 K]. PS(h) = 7.5 kg·mol^{-1}/acetone solutions are well removed from the hypercritical region for all values of y_D. The well behaved linearity establishes the acetone-h/acetone-d solvent mixture as ideal (within experimental precision) according to Singh and Van Hook.[33] The upper curve refers to PS(h) = 13.5 kg·mol^{-1} and is of more interest; it shows a good deal of curvature. This solution has its hypercritical point near y_D = 1, and has been diagrammed in the (T,W_{ps}) plane at various pressures (Figure 3, middle sequence). Figure 8 illustrates the solvent isotope dependence of T_c as the hypercritical point is approached at constant P, W_{ps}, MW, and ϱ_m. As $|T - T_{hcp}| \rightarrow 0$, $(\partial T_{cr}/\partial y_D)_{P,MW,\varrho MW}$ becomes unbounded in strict analogy to the behavior in the (T,P) plane where $(\partial T_{cr}/\partial P)_{y_D,MW,\varrho MW}$ also becomes unbounded as T_{hcp} is approached. At any particular isotope ratio, y_D, the solvent IE can be written

$$T_{cr}(y_D) = T_{cr}(y_D = 0) + \int(\partial T_{cr}/\partial y_D)\, dy_D \qquad (5)$$

In the sense that $(\partial T_{cr}/\partial y_D)$ gets very large (but only in the vicinity of T_{hcp}), the solvent isotope effect, $\Delta T_{cr,ucs}$ = [$T_{cr}(y_D = 0) - T_{cr}(y_D = 1)$] may be said to be hypercritically enhanced. While large curvature in the (T_{cr},y_D) suggests large nonideality of the solvent isotopomer mixture in the Singh–Van Hook sense,[33] that interpretation likely does not apply in the near-critical region. Well removed from T_{hcp}, *i.e.* for small y_D, $\partial T_{cr}/\partial y_D$ is almost the same for PS(h) = 13.5 kg·mol^{-1} as it is for PS(h) = 7.5 kg·mol^{-1}. Table 6 reports parameters of fit for the two sets of data extending across the entire

Table 6. Critical T–y_D Dependence[a]

polymer	β	A	B	10^3C	T_{hcp}/K	$y_{D_{hcp}}$	$10^3\sigma$
			$y_D = A + BT + CT^2$ (eq 6)				
PS(h)-7.5		−7.67223(0.0023)	0.030248(9.7 × 10^{-5})				2.31
PS(h)-13.5		−23.5379(0.017)	0.137063(5.8 × 10^{-3})	−0.19137(8.8 × 10^{-3})			17.1
			$t^* = A_{y_D}y_D^{*\beta} + B_{y_D}y_D^{*\beta+1/2}$ [b]				
PS(h)-13.5	1/2	0.20196(0.0049)			358.12	1.0046	6.79
	1/3	0.178062(0.0115)			358.12	1.0046	17.9
	1/3	0.10692(0.0107)	97.365(13.6)		358.12	1.0046	5.86

[a] Parameters of fit of scattering data for some PS(h) + y_D(CD$_3$)$_2$CO + (1 − y_D)(CH$_3$)$_2$CO) solutions at the critical composition (W_{ps}(cr)). p = 0 for PS-7.5 kg·mol^{-1} and p = 0.5 MPa for PS-13.5 kg·mol^{-1} (range 0 < y_D < 1). Values in parentheses report the standard error. [b] Note: $|T^*| = |1 - T/T_{hcp}|$, $y_D^* = (1 - y_D/Y_{D_{hcp}})$.

span of y_D (Figure 8). Each data set is fit with eq 6.

$$y_D = a_0 + a_1T_{cr} + a_2T_{cr}^2 \quad (6)$$

Two terms sufficed for PS(h) = 7.5 kg·mol^{-1}; PS(h) = 13.5 kg·mol^{-1} required three. We also fit the data for PS(h) = 13.5 kg·mol^{-1} with one and two parameter scaling relations (eq 7), writing $y_D^* = |1 - y_D/y_{D,hcp}|$ and $t^* = |1 - T/T_{hcp}|$. β, the scaling exponent, was fixed as 1/3 (nonclassical) or 1/2 (mean-field),

$$t^* = [A_{y_D}y_D^{*\beta} + (c_{y_D}A_{y_D}/T_{hcp})y_D^{*(1+\beta)})] \pm (c_{y_D}/T_{hcp})y_D^*$$
(positive for $T > T_{hcp}$, negative for $T < T_{hcp}$) (7)

and T_{hcp} was picked from plots of the data. Results are in Table 6. For the data in Figure 8 the skewing term, $(c_{yD}/T_{hcp})y_D^*$, is not required because not many points lie along the high-temperature branch. Clearly eq 7 fits the data as well as eq 6.

4.3. Molecular Weight Dependence of Critical Demixing. UCS and LCS cloud points for PS(h) in (CH$_3$)$_2$CO or MCP(h) from this and the earlier study,[1] as well as data reported by Cowie and McEwen[34] for MCP(h) solutions, all extrapolated or interpolated to P = 0.5 (acetone) or 0 MPa (MCP), are listed in Table 7 and plotted *vs* (1/MW) in Figures 9a and 9b. The results of Patterson *et al.*[16] for PS(h)/(CH$_3$)$_2$CO are consistent with the present data, but scatter more widely and are not shown. Previous authors have elected to interpret UCS or LCS data using the Schultz–Flory relation.[29] For systems with a hypercritical point, Schultz–Flory plots display marked curvature.[16,17,34] In the following we elect an alternate scaling representation, extending a suggestion of Van Hook.[35]

Figure 9a shows (T_c,MW^{-1}) demixing data for PS(h)/(CH$_3$)$_2$CO, PS(d)/(CH$_3$)$_2$CO, PS(h)/(CD$_3$)$_2$CO, and PS(d)/(CD$_3$)$_2$CO solutions. Almost all of the data are for PS(h) dissolved in (CH$_3$)$_2$CO or in (CD$_3$)$_2$CO, because the high cost of deuterated polymer prohibited the purchase of more than two PS(d) samples. The shapes of the PS(h)/(CH$_3$)$_2$CO and PS(h)/(CD$_3$)$_2$CO curves are well-defined by the experiments. We choose to fit the data to eq 8. (1/MW)* is a fitting parameter introduced below.

$$t^* = [A_{MW}(1/MW)^{*\beta} + (c_{MW}A_{MW}/T_{hcp})(1/MW)^{*(1+\beta)})] \pm (c_{MW}/T_{hcp})(1/MW)^*$$
(positive for $T > T_{hcp}$; negative for $T < T_{hcp}$) (8)

The fits to eq 8 are plotted as the solid and dashed lines in Figures 9a and 9b. We chose β = 1/3 and used T_{hcp} as graphically determined. (Trial fits with β = 1/2 gave a poorer representation and were rejected.) The skewing parameter in this projection is small and it is possible to fit the data for acetone *almost* within experimental precision using $c_i = 0$. For MCP solutions the skewing parameter is not required. Least squares parameters are reported in Table 8.

Table 7. LCS and UCS Binodal Transition Temperatures Corrected to (a) Zero Pressure for Some Polystyrene/MCP Solutions and (b) p = 0.5 MPa for Some Polystyrene/AC Solutions[a]

system	y_D; z_D	T_{ucst}/K	T_{Lcst}/K	10^5MW^{*-1}/g^{-1}·mol	ref
B + acetone	0; 0	253.68			*
	0.546; 0	271.64			*
	0.669; 0	275.70			*
	1; 0	286.77			*
D + acetone	0; 0	285.34			*
	0.483; 0	307.13			*
	0.719; 0	318.81			*
	0.952; 0	341.54	372.21		*
	1; 0	350.32	367.34		*
acetone	0; 0	227	486	40.0	1, 14
		245	458	20.0	1, 14
		251	452	17.2	1, 14
		253.3	442	13.3	1, 14, *
		260	437	12.5	1, 14
		274.8	421	8.62	1, 14, *
		285.3	400	7.4	1, 14, *
		341.2	351.7	4.5	*
	1; 0	259	444	20.0	1, 14
		270	436	17.2	1, 14
		286.1	428	13.3	1, 14, *
		282	420	12.5	1
		350.3	367.3	7.4	*
	1; 1	269.2		9.52	*
	0.50; 0	350.0		3.70	*
	0; 1	235.7		9.52	*
		279		3.70	*
MCP	0; 0	259.69		25.0	*
		291.93		7.4	*
		300.94		4.5	*
		303.65		4.00	*
		327.52		0.943	*
		255	508	40.0	1, 14
		268	500	20.0	1, 14
		270	492	13.3	1, 14
		294	480	8.62	1, 14
		322	445	0.909	34
		329	438	0.418	34
		338	428	0.116	34
		342	422	0.050	34
	1; 0	310.07		4.00	*
		339.41		0.943	*
	0; 1	303.48		3.70	*
	1; 1	308.90		3.70	*

[a] See Tables 2, 6, 8, and 9. [b] * = this work.

For PS(h) solutes in either or acetone-h or -d there are sufficient data to define all parameters, T_{hcp}, MW$_{hcp}^{-1}$, A_{MW}, and c_{MW} (see Figure 9, Table 8). Solvent IE's on MW$_{hcp}^{-1}$ and T_{hcp} are significant, ((MW$_{hcp}^{-1}$)$_h$ − (MW$_{hcp}^{-1}$)$_d$)/(MW$_{hcp}^{-1}$)$_h$ ≈ −0.63 and $\Delta T_{hcp}/T_{hcp}$ = −0.03,

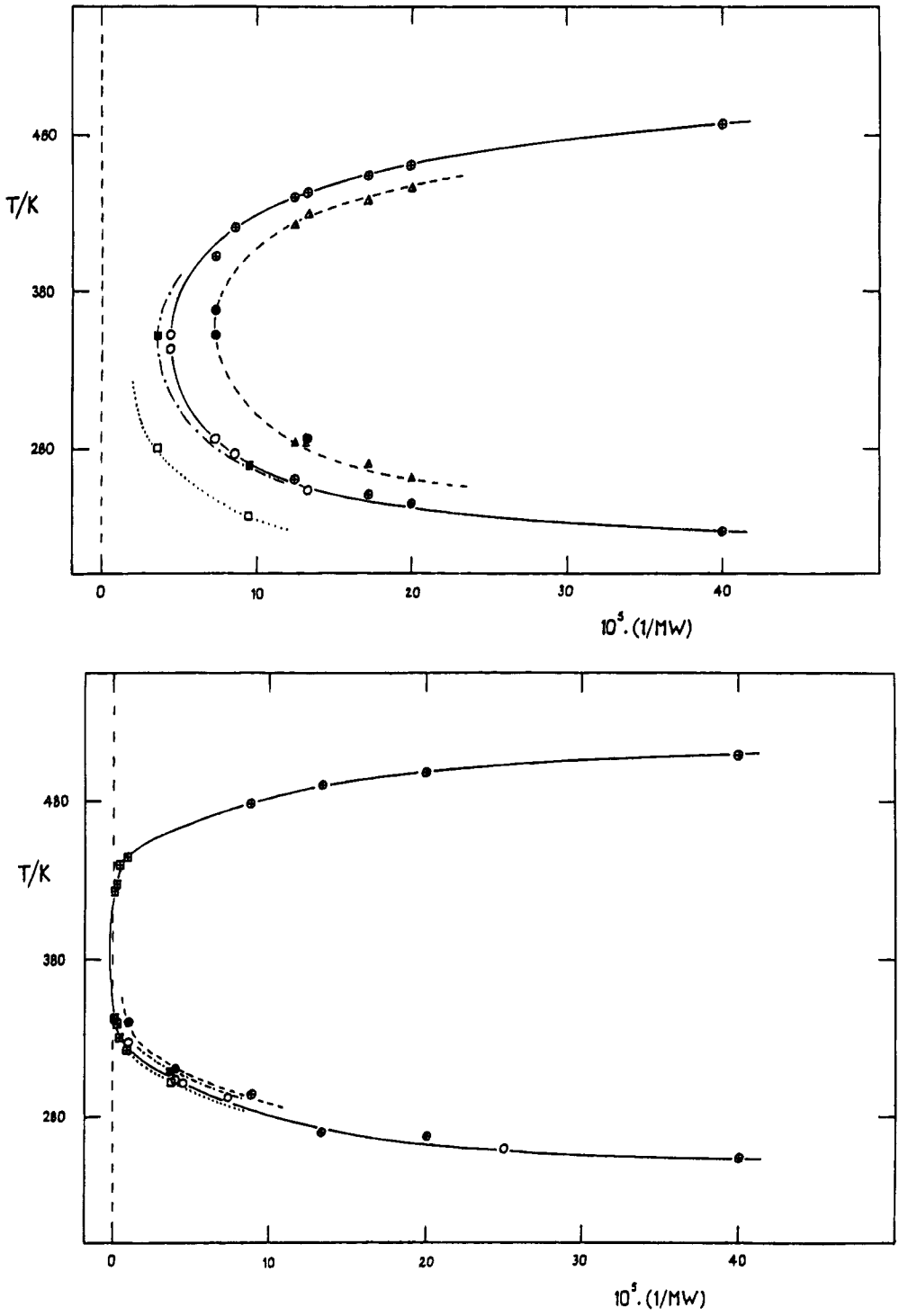

Figure 9. Molecular weight and solvent and solute isotope dependence of UCS and LCS transition temperatures. (a) Upper (0.5 MPa): (—) PS(h)–$(CH_3)_2CO$; (···) PS(d)–$(CH_3)_2CO$; (- - -) PS(h)–$(CD_3)_2CO$; (— · —) PS(d)–$(CD_3)_2CO$; ■, □, ●, ○, this work; ⊕, △, ref 1. (b) Lower (0 MPa): (—) PS(h)–MCP(h); (···) PS(d)–MCP(h); (- - -) PS(h)–MCP(d); (— · —) PS(d); ■, □, ○, ○, this work; ⊕, ref 1; □, ref 34.

but the former are relatively much larger and predominate; they are hypercritically enhanced. The PS(h/d) solute IE is still large, $\Delta MW^{-1}/MW^{-1} = 0.5$, $\Delta T_{hcp}/T_{hcp} \approx 0.02$, but notice the sign change as compared to the solvent IE.

We could only afford two deuterated polymer samples and have elected to fit data for those solutions in acetone-h_6 by lumping the isotopic difference, PS(h) – PS(d), into the MW_{hcp}^{-1} parameter. To do so we assumed the solvent IE on T_{hcp} for PS(d) in $(CH_3)_2CO$ was the same as that for PS(h). UCS loci so calculated fit the data within the experimental error (dotted and dash-dotted lines in Figure 9).

The largest IE's, ΔMW_{hcp}^{-1} and ΔT_{hcp}, are negative for H/D substitution on the solvent and positive for H/D substitution on the polymer. Solute and solvent H/D IE's, while the opposite sign, are of comparable magnitude (Table 8). That observation is important when correlating these thermodynamic isotope effects with vibrational properties (see below).

Figure 9b shows demixing data for MCP solutions in the (T_c,MW^{-1}) plane. MCP is a much better solvent for PS than acetone, and the miscibility window extends to infinite molecular weight.[34] Even so we still chose

Table 8. Critical T − 1/MW Dependence[a]

solvent	y_D; z_D	β	A_{MW}	B_{MW}	c_{MW}	T_{hcp}/K	$(10^5/MW)_{hcp}$	$10^3\sigma$
MCP[b]	0; 0	1/3	1.40029(0.024)	−2.17544(0.159)		383.7	−0.52	8.23
AC	0; 0	1/3	1.363827(0.037)	−1.37264(0.27)	278.371(31.0)	346.491(0.91)	4.544	10.9
	1; 0	1/3	1.094573(0.013)		−576.924(104.9)	359.38(1.04)	7.3975	7.8
	0; 1	1/3	1.346(- -)			344.8	1.18	(- -)
	1; 1	1/3	1.231(- -)			350.0	3.70	(- -)

[a] Parameters of fit of scattering data for some PS(h) + MCP(h) and PS(h) + Ac(h), PS(h) + AC(d), PS(d) + Ac(h), and PS(d) + Ac(d). Values for MCP were taken at zero pressure and for acetone at p = 0.5 MPa. $|t^*| = A_{MW}(1/MW^*)^{\beta} + B_{MW}(1/MW^*)^{\beta+1/2} + (c_{MW}A_{MW}/T_{hcp})(1/MW^*)^{\beta+1} + (c_{MW}B_{MW}/T_{hcp})(1/MW^*)^{\beta+1.5} \pm (c_{MW}/T_{hcp})(1/MW)$; (positive for $T > T_{hcp}$, negative for $T < T_{hcp}$) (eq 32).[c] Range $0 < 1/MW^* < 0.04$. Values in parentheses report the standard error. [b] θ_{ucs} = 338.6 K; θ_{lcs} = 428.8 K (for $\beta = 1/2$). θ_{ucs} = 341.4 K; θ_{lcs} = 426.0 K (for $\beta = 1/3$). [c] Note: $|t^*| = |1 - T/T_{hcp}|$, $(1/MW^*) = (1 - [(1/MW^\circ - 1/MW)/(1/MW^\circ - 1/MW_{hcp})]$ with MW° = 104 g·mol^{-1} for $z_D = 0$ and MW° = 112 g·mol^{-1} for $z_D = 1$.

to fit the data to eq 8, as before regarding MW_{hcp}^{-1} as the fitting parameter, but this time extending into the negative domain. A proper fit of the MCP data requires a two term expansion because of the marked curvature at high molecular weight. The MW^{-1} intercepts of these fits yield upper and lower Θ points of 426 and 341 K, which compare favorably with the values obtained by Cowie and McEwen[34] (417 and 348 K). Isotope effects for the PS−MCP solutions are of the same sense as the IE's for PS−acetone but are significantly smaller in magnitude for both solute and solvent deuteration (Table 7 and Figure 9b). In comparing Figures 9a and 9b, it is interesting to note that at low MW and low temperature acetone is a better solvent than MCP but the curves cross at intermediate MW and temperature; thereafter MCP is the better solvent.

5. Interpretation

In the remaining sections we address important questions of interpretation, including (i) the effect of molecular weight dispersion on the phase diagrams for solutions of interest to us ($\varrho_m < 1.2$), (ii) the representation of the phase equilibrium data as functions of T, P, MW, ϱ_m, z_D, and y_D using multidimensional scaling or mean-field representations, and (iii) the connection between the present observations and the theory of isotope effects in condensed phases.[2-4]

5.1. Effect of MW Fractionation on Cloud-Point and Coexistence Curves. 5.1a. General Information. The equilibrium condition based on equating partial molar free energies of the monodisperse solvent, μ_A, and each individual polymer species in a polydisperse sample of solute, $\mu_{B,i}$, may be specified in terms of eqs 9−11. The variables have been defined in an earlier section. $W_{B,i}(r)$ is the polymer segment distribution function for phase i. The equations presuppose the introduction of r as a continuous variable. An equation of type (9) can be written for every value of r.

$$\Delta\mu_{B,r} = (\mu_{B,r,2} - \mu_{B,r,1}) = 0 = \Delta\mu_{B,r}(T,P,\psi_1,\psi_2,r_{n,1},r_{n,2},\varrho_{m,1},\varrho_{m,2},y_{D,1},y_{D,2},z_{D,1},z_{D,2}) \quad (9)$$

$$\Delta\mu_A = (\mu_{A,2} - \mu_{A,1}) = 0 = \Delta\mu_A(T,P,\psi_1,\psi_2,r_{n,1},r_{n,2},\varrho_{m,1},\varrho_{m,2},y_{D,1},y_{D,2},z_{D,1},z_{D,2}) \quad (10)$$

$$\int W_{B,1}(r)\,dr = \int W_{B,2}(r)\,dr = 1 \quad (11)$$

5.1b. Two Component Monodisperse Solution. Treatments of precipitation from solutions of monodisperse polymers at natural isotopic abundance are commonly available. Here, $\langle r\rangle_{n,1} = \langle r\rangle_{n,2} = r$ and $\varrho_{m,1} = \varrho_{m,2} = 1$. The angular brakets, $\langle\ \rangle$, denote averages. Also $y_{D,1} = y_{D,2} \approx 0$ and $z_{D,1} = z_{D,2} \approx 0$. Thus, $\Delta\mu_i = 0 = \Delta\mu_i(T,P,\psi_1,\psi_2,r,\varrho_m = 1, y_D = 0, z_D = 0)$; CP and BIN necessarily coincide. At precipitation $\psi_2 \neq \psi_1$, but only an infinitesimal amount of phase 2 forms, so ψ_1 remains unchanged. Thus BIN can be mapped by performing a series of CP experiments. It is not necessary to determine ψ_2 because experiments vary ψ_1 across the range of interest.

5.1c. A Polydispersity Example with $\Delta\varrho_m = 0$. We review a simple model for polydisperse phase equilibria. Consider a precipitation characterized by $\langle r\rangle_{n,1} \neq \langle r\rangle_{n,2}$, but $\varrho_{m,1} = \varrho_{m,2}$, and $y_D = z_D = 0$. The conditions are satisfied for Schulz−Flory distributions.[20] The CP constraint becomes

$$\Delta\mu_i = 0 = \Delta\mu_i(T,P,\psi_1,\psi_2,\langle r\rangle_{n,1},\langle r\rangle_{n,2})_{\varrho_m,y_D=0,z_D=0} \quad (12)$$

It is convenient to further restrict the number of variables and consider the phase diagram in $(\eta,\psi,r)_{\eta',\varrho_m,y_D,z_D}$ space. In the example η might be either T or P, and η' its sister variable, P or T, respectively. For the moment drop subscripts y_D and z_D (restricting attention to natural abundance) and consider $(T,\psi,r)_{P,\varrho_m}$ space. Transformation to $(P,\psi,r)_{T,\varrho_m}$ is straightforward. A schematic coexistence diagram in $(T,\psi,r)_{P,\varrho_m}$ space is shown in Figure 10a. It is useful, although not completely accurate, to approximate the diagram as a series of coexistence curves (T *vs* ψ, at constant r_i), each separately constructed using BIN. Four such projections are sketched in Figure 10a. We elect a reference curve, r_i. Of the three other curves, one lies at $r_h < r_{i,o}$, the others at $r_j > r_{i,o}$ and $r_k > r_j$. The projections at r_h, r_i, and r_j show upper and lower branches and consolute points, the one at r_k lies above the hypercritical segment number, r_{hcp}, and is in the hourglass configuration (r_{hcp} may depend on P, ϱ_m, y_D, and z_D and is more completely specified as $r_{hcp,T,\psi,P,\varrho_m,y_D,z_D}$). Were one to begin with a homogeneous monodisperse parent solution with segment number and concentration $(r_{i,o}, \psi_1)_{P,\varrho_m,y_D,z_D}$, and lower or raise the temperature to induce precipitation, points A and B, and A′ and B′, would show the (T,ψ) coordinates of coexisting parent and daughter phases in the upper consolute solutions (UCS) and lower consolute solution (LCS) branches. However our interest is in polydisperse samples where MW fractionation must be considered. Beginning with a polydisperse parent solution of average segment number and concentration $(\langle r\rangle_i,\psi_1)$, the parent solution at point A is now in equilibrium with the daughter (shadow, SHDW) solution at a different concentration and different $\langle r\rangle$, at say point C. Also $\psi_{2,C} > \psi_{2,B}$. The tie line which connects $(T_1,P_1,\psi_1,r_{1,i})$ and $(T_2,P_2,\psi_2,r_{2,j})$ does not lie in the $(T,\psi)_{r_i,o}$ plane but angles across the $(\psi,r)_{T,P,y_D,z_D}$ plane. Similarly, a parent (CP) solution initially at B will equilibrate with daughter (SHDW) solution at a lower $\langle r\rangle$ value, say at D, where $\psi_{2,D} < \psi_{2,A}$. The same

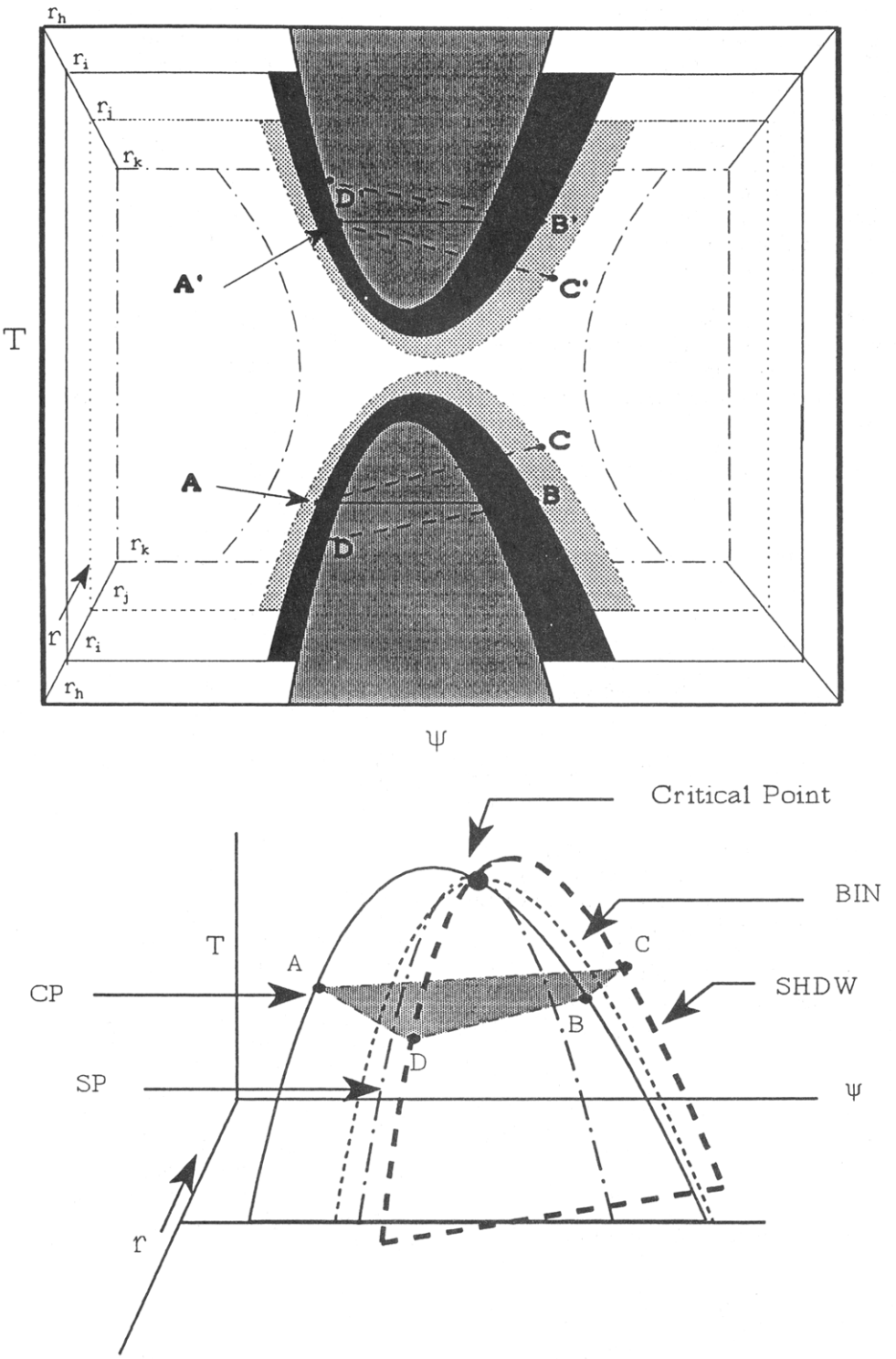

Figure 10. (a) Schematic showing UCS/LCS demixing in (T,ψ,r) space. ψ is the segment fraction of polymer, and r is the segment number. Four (T,ψ), projections are shown. Three, (the (T,ψ) projections at r_h, r_i, and r_j), are in the LCS/UCS configuration, the projection at r_k has dropped into the hourglass configuration. Consider a parent solution with average segment number $\langle r\rangle_{i,o}$. In the monodisperse approximation the coexisting phases are labeled A and B (UCS branch), and A′ and B′ (LCS branch). There is no $\langle r\rangle$ fractionation on precipitation. For polydisperse samples fractination in $\langle r\rangle$ occurs, the equilibrating solutions for low polymer concentration in the parent solution are labeled A and A′ (parent) and C and C′ (SHDW), and for high polymer concentration in the parent they are labeled B and B′ (parent) and D and D′ (SHDW), as shown with the dashed tie lines. The fractionation in $\langle r\rangle$ which occurs on precipitation is apparent. Projections in (T,ψ,P), (T,ψ,y_D), and (T,ψ,z_D) space are analagous. Compare with Figure 1. (b) Schematic cloud point (CP), spinodal (SP), and shadow (SHDW) curves, compared with the monodisperse (BIN) approximation for a UCS type solution. Heavy solid curve = CP. Heavy dashed curve = SHDW. Lightly dashed curve = BIN. Dash-dot curve = SP. CP, SP, and BIN lie in a common (T,ψ) projection at constant $\langle r\rangle_n$. SHDW is skewed and projects a diagonal onto the (r,ψ) plane. The four curves are common at the critical point.

kind of analysis obtains for the LCS branch where the equilibrating solutions are labeled A′ and C′, B′ and D′. The features which most concern us are CP, SHDW, SP, and BIN, and these are illustrated for the UCS case in Figure 10b. That figure is discussed in a following section.

Should one continue to lower the temperature beyond B, or raise it above B′ (Figure 10a or 10b), more and more of phase 2 would precipitate, and $\langle r\rangle$ for both parent and daughter phases would fall from their initial values because higher r fractions precipitate first. For a finite excursion into the heterogeneous region the coexistence equilibrium is between two new phases with $\langle r\rangle_1 \neq \langle r\rangle_2 \neq \langle r\rangle_0$. That is not our present concern. In the paragraphs below we describe the results of calculations of liquid−liquid phase diagrams (CP, SHDW, and SP profiles) limiting analysis to the case of infinitesimal precipitation.

5.2. Some Calculations Based on Continuous Thermodynamics. 5.2a. Cloud Point and Shadow Curves. Ratzsch and Kehlen (RK)[20] have written expressions for the chemical potential per segment for solvent (A) and polymer (B) species:

$$\mu_A/r_A = \mu_A^* + Rt[\ln(\psi_A)/r_A + 1/r_A - 1/r^\ddagger] + RT \ln f_A \quad (13)$$

$$\mu_B(r)/r = \mu_B(r)^* + RT[\ln(\psi_B W_B(r))/r + 1/r - 1/r^\ddagger] + RT \ln f_B(r) \quad (14)$$

Here r_A is the segment number for solvent, r the segment number for a particular polymer species, $\psi = \psi_B = (1 - \psi_A)$, and the μ^*'s are standard state partial molar free energies.

$$(1/r^\ddagger) = (1 - \psi)/r_A + \psi/r_B^\ddagger \qquad 1/r_B^\ddagger = \int (W_B(r)/r)\, dr \quad (15)$$

The segment molar activity coefficients f_A and $f_B(r)$ may depend on T, P, ψ, $W_B(r)$, and r. A common choice is to assume the excess free energy is of the Redlich−Kister form, $G^{ex}/R = \psi(1 - \psi)[\xi(T,P,\psi,...)]$, $\xi(T,P,\psi,...) = \chi_0(T,P,...) + \chi_1(T,P,...)(1 - 2\psi) + ...$ For a one term expansion, $\ln(f_A) = \chi_0(T,P)\psi^2/r_A$ and $\ln(f_B) = \chi_0(T,P)(1 - \psi)^2/r$. It is this form which is used below until otherwise qualified. For the daughter phase (SHDW, subscript 2),[20]

$$(1/r_2^\ddagger) = (1 - \psi_2)/r_A + \int (\psi_1 W_{B,1}(r)/r) \exp(r\zeta_B(r))\, dr \quad (16)$$

where

$$\zeta_B(r) = 1/r_2^\ddagger - 1/r_1^\ddagger - \ln(f_{B,2}(r)) + \ln(f_{B,1}(r)) \quad (17)$$

$$\zeta_A = 1/r_2^\ddagger - 1/r_1^\ddagger - \ln(f_{A,2}) + \ln(f_{A,1}) \quad (18)$$

If the excess free energy of the solution, G^E, is independent of $W_B(r)$, $\zeta_B(r) = \zeta_B$. For

$$W_{B,1}(r) = (h^{(h+1)}/(r_{B,1}^\ddagger \Gamma(h + 1))(r/r_{B,1}^\ddagger)^h \exp(-hr/r_{B,1}^\ddagger) \quad (19)$$

which is the generalized Schulz−Flory distribution, eq 16 yields

$$\psi_2/\psi_1 = (r_{B,2}^\ddagger/r_{B,1}^\ddagger)^{(h+1)} \quad (20)$$

$W_{B,2}(r)$ is a Schulz−Flory distribution with $h_2 = h_1 = h$ and $r_{B,2}^\ddagger/r_{B,1}^\ddagger = 1 - r_{B,1}^\ddagger\zeta_B/h$. CP and SHDW are calculated using eqs 14−20 provided f_A and $f_B(r)$ are known (*vide supra*). In eq 19 $1/h = (\varrho_m - 1)$. $\Gamma(h + 1)$ is the gamma function.

5.2b. Spinodal Locus for the Parent Solution. The SP locus can be evaluated from the condition $(\partial^2 G/\partial\psi^2) = 0$. For the monodisperse solution the result is well-known.[24]

$$1/(r_A(1 - \psi)) + 1/(\psi\langle r\rangle_w) + (\partial^2/\partial\psi^2)[G^{ex}/(RT)] = 0 \quad (21)$$

For polydisperse solutions eqs 13 and 14 may be used to calculate the total free energy:

$$G^\ddagger/RT = [G - ((1 - \psi)\mu_A^* + \psi\sum W_B(r) r\mu_B(r)^*)]/RT = (1 - \psi)\ln(1 - \psi) + (1 - \psi)(1 - 1/r^\ddagger) + (1 - \psi)\ln(f_A) + \sum[\psi W(r)\ln(\psi W(r)) + \psi W(r)(1 - r/r^\ddagger + W(r)\psi \ln(f_B)] \quad (22)$$

where we have taken $r_A = 1$. Until otherwise qualified we will continue to set $r_A = 1$. For the Schultz−Flory distribution the spinodal locus is the same as that for the monodisperse solution because both $W(r)$ and r are independent of ψ.

5.2c. Calculations: Cloud, Shadow, and Spinodal Curves. Using eqs 13−21, we have made calculations of CP, SHDW, and SP curves for Schultz−Flory solutions at concentrations and temperatures not too far from critical, for $(12.5 \leq \langle r\rangle_n \leq 1250)$ and $(1 \leq \varrho_m \leq 1.5)$. Previous authors paid little or no attention to solutions of small MW and low ϱ_m.

To calculate CP and SHDW we wrote two different programs employing different algorithims (to check numerical methods). The first, given (ψ_1, r_1, ϱ_m) and initial guesses for ψ_2 and G^E/RT, $G^E = G^E(T,P,\psi,r,y_D,z_D)$, solves eq 20 for r_2, substitutes the result into eq 10, then searches for that ψ_2 with $\Delta\mu_A = 0$, keeping G^E/RT at the initially guessed value, finally testing $\Delta\mu_B$ (eq 9). If $\Delta\mu_B \neq 0$, G^E/RT is incremented and the routine continues until $\Delta\mu_A = \Delta\mu_B = 0$. Although straightforward in outline, the procedure is tedious to implement because the free energy minima are extremly shallow, especially near extrema. Phase equilibrium loci are easily missed if the increment net is chosen too large, or if the initial estimates of ψ_2 and/or G^E/RT lie too far from equilibrium. Even so, with care, the method yields useful phase equilibrium data. The second procedure is much more efficient. Once again eq 20 is solved for r_2 which is eliminated from eqs 10 and 23 (eq 71 of RK).[20]

$$\Delta\zeta = [(h/\langle r_{B,2}\rangle) + 1/r_{B,2}^\ddagger - \ln(f_{B,2})] - [(h/\langle r_{B,1}\rangle) + 1/r_{B,1}^\ddagger - \ln(f_{B,1})] = 0 \quad (23)$$

Equations 10 and 23 are summed; the result is solved for the zero roots. In the two-phase region three roots are observed. Solution sets are examined for a particular choice of ψ as a function of G^E/RT using eq 23; the program selects a particular G^E/RT which approximately satisfies the Maxwell equal area criterion. That original approximate solution is then refined by iterating eq 23 over small steps in ψ_1 at constant G^E/RT (or small steps in G^E/RT at constant ψ_1, as appropriate) until convergence is obtained subject to the observation of zero roots for eqs 10 and 23 and their sum. The method gives results in quantitative agreement with the earlier search routine but the process is more than ten times faster and can be employed at higher numerical precision. The resulting computer algorithim[36] has been

Table 9. Critical T–P Dependence[a]

system	y_D; z_D	β	A_p	B_p	c_P	T_{hcp}/K	P_{hcp}/MPa	$10^3\sigma$
E	0; 0	1/2	0.364776(0.002)		83.0628(1.85)	346.28(0.06)	0.429	0.89
D	1; 0	1/2	0.346928(0.002)		85.0053(2.79)	356.86(0.08)	0.3161	1.16
XE + (1 − X)D	0.5; 0	1/2	0.351215(0.002)		86.4770(2.33)	354.49(0.04)	1.480	0.71
I	1; 1	1/2	0.357762(0.003)		93.9586(1.76)	351.10(0.04)	2.617	0.99

[a] Parameters of fit of scattering data for some (PS + Ac) systems at the critical concentration, W_{ps}(cr). Values in parentheses report the standard error of each parameter. $|t^*| = A_P P^{*\beta+1/2} + (c_P A_P/T_{hcp})P^{*\beta+1}$ $(c_P B_P/T_{hcp})P^{*\beta+1.5} \pm (c_P/T_{hcp})P^*$; (positive for $T > T_{hcp}$, negative for $T < T_{hcp}$).[b] [b] Note: $|t^*| = |1 - T/T_{hcp}|$, $p^* = (1 - [(40 - P)/(40 - P_{hcp})])$, P in MPa; $0 < p^* < 0.07$.

labeled PHASEEQ[r] and is coded in QUICKBASIC[r]. The solution of eq 21 for SP is straightforward. Mumby, Qian, Sher, and Eichinger[37,38] have recently described calculations of phase diagrams for quasi-binary solutions of polymers and blends and using methods developed by Solc and others[39–41] and have applied it to multicomponent mixtures (*i.e* to mixtures of quasi-binary mixtures, in one case[40] containing five components). Another approach has been described in exhaustive detail by Kamide.[42] Finally, Hue, Ying, Wu, and Prausnitz[43] have reported on a continuous thermodynamic model based on the Freed[44] theory of polymer solutions. They demonstrated the method with calculations of UCS (lower branch) demixing diagrams for high MW samples with $\varrho_m > 2$ and did not investigate the hypercritical region or the upper branch. All these methods differ in essential detail from the present approach.

5.3. Results of Calculations. 5.3a. Initial Results. In preliminary calculations designed to quantify the effects of polydispersity on CP and SHDW we chose the FH free energy parameter χ to be a constant independent of ψ and other variables, ($\chi = \chi_o$), and considered UCS phase diagrams only. By this technique we reduce the problem to its simplest terms. Later it will be necessary to treat more complicated cases and consider χ as $\chi(T,P,\varrho_m,y_D,z_D)$. Calculations were made at $\langle r\rangle_n$ = 12.5, 125, and 1250, and $1 \le \varrho_m \le 1.5$. Approximately 50 coexistence points were calculated for each ($\langle r\rangle_n,\varrho_m$) set yielding CP, SP, and SHDW curves and [$\langle r\rangle_{n,CP}/\langle r\rangle_{n,SHDW}$] fractionations. Also we calculated BIN for the corresponding monodisperse approximation. For economical representation of the results we least squares fit them to Wegner-type expansions[45] centered on the *maxima* of the various curves.

$$\psi = B_0 + B_1|t^\ddagger| + B_2|t^\ddagger|^{1-\alpha} + B_3|t^\ddagger|^{1-\alpha+\Delta} + (f/2)\sum C_i|t^\ddagger|^{\beta+i\Delta} \quad (24)$$

In eq 24 $t^\ddagger = (T_{max} - T)/T_{max}$ and is different than the commonly employed reduced temperature, $t^* = (T_{cr} - T)/T_{cr}$. Also $\Delta = 0.5$, $\alpha = 0$, $\beta = 1/2$, $B_3 = 0$, and $f = -1$ if $\psi < B_0$ and $f = 1$ if $\psi > B_0$. The least squares parameters are reported in Table 10.

The most important features of the calculated UCS diagrams are illustrated in Figure 10b which is a three-dimensional $(T,\psi,r)_{P,y_D,z_D}$ schematic representation of CP, SHDW, and SP for $\varrho_m \approx 1.5$ (exaggerated in order to more clearly illustrate the effects of MW dispersion; experiments were limited to $1.02 \le \varrho_m \le 1.09$). In Figure 10b the solid curve represents CP (parent), and the heavy dashed curve shows SHDW (daughter). Solutions with $\psi_1 < \psi_c$ give SHDW fractionated to $r_2 > r_1$ and $\psi_2 > \psi_1$ (tie line AC for example); those with $\psi_1 > \psi_c$ give SHDW fractionated to $r_2 < r_1$ and $\psi_2 < \psi_1$ (tie line BD for example). The CP (solid line) and SP curves (dash-dot) each lie in the $(T,\psi)_r$ plane, as does BIN (light dashed), but SHDW is rotated out of that plane (see figure, and compare with Figure 10a). The critical point, (T_c,ψ_c), is assigned to the intersection of CP and SHDW. At that point SP and CP are tangent. The SP curve characterized by ($\langle r\rangle_n,\varrho_m$) is coincident with that for a monodisperse polymer with $1/r^{BIN} = \langle 1/r\rangle_n(1/\varrho_m) = \langle 1/r\rangle_w$. The monodisperse demixing curve, BIN, for $r = \langle r\rangle_w$ is also shown. BIN lies in the $\langle r\rangle_n$ plane and shows incident CP and SHDW branches. All four curves, CP, SHDW, SP, and BIN are common at (T_c,ψ_c), and this criterion can be used to test the precision of the calculations. We find the maxima in BIN and SP to coincide with the intersection of CP and SHDW within 0.001 ψ unit and 0.1 K or so, except for samples with $\varrho_m \ge 1.3$ where the differences are greater. The error is accounted for by round-off and/or truncation in subroutines involving averaging over broadened SF distributions. In any case computational precision is well within our requirements, and for samples with $\varrho_m \le 1.1$ exceeds experimental precision.

Figure 11 illustrates the effects of polydispersity and of higher order terms in the concentration expansion on calculated demixing curves in the UCS regime. Figure 11a demonstrates the importance of polydispersity by plotting calculated CP and SHDW for two different values of ϱ_m, choosing $\langle r\rangle = 125$ and $\chi_{0,0} = 2000$ J·mol^{-1} in a one term expansion of G^{ex} (see below). For these conditions the difference in calculated T_c's is about 10 K. The upper curves are for $\varrho_m = 1.5$; the lower, for $\varrho_m = 1.05$. In each case BIN lies between CP and SHDW but closer to CP. The CP–SHDW and CP–BIN differences (the latter not included in the figure) increase markedly with ϱ_m.

Figure 11b examines the effect of higher order terms in the concentration expansion. We choose $\langle r\rangle = 240$ and generate CP and SHDW curves by picking χ parameters to yield maxima in the calculated UCS curves which agree with experiment for the particular MCP/PS solution specified in the caption (experimental data points are shown). The left-hand curves with $\chi_{0,0}$ = 1425 J·mol^{-1} (for a one term expansion of G^{ex}) are found at much too low ψ, and show too much curvature. The addition of a higher order term of the proper sign, *i.e.* now setting $\chi_{0,0} = 2039.5$ and $\chi_{1,0} = -248.4$ J·mol^{-1} (all other parameters zero), moves the maximum toward higher concentration and broadens the CP curve into good agreement with experiment. The alternate choice, *i.e.*, taking $\chi_{1,0}$ positive, has the opposite effect. It sharpens the CP curves and moves the maximum to lower ψ. The result is typical; it demonstrates yet again that the one term, zero order, FH expression is inadequate to rationalize the concentration dependence of demixing.

In Figure 12 we further explore fractionation and other effects in Schultz-Flory solutions. The maximum in CP is always found at $T_{CP,max} > T_c$ and $\psi_{CP,max} < \psi_c$ (Figures 10 and 11). We continue to represent the effects of polydispersity as straightforwardly as possible by considering the one term zero order theory. Numeri-

Table 10. Coefficients of Eq 24

ϱ_m		T_{max}	Ψ_{max}	B_0	B_1[a]	B_2[a]	C_0	C_1	σ
					$\langle r\rangle = 12.5$				
1.01	BIN	292.979	0.2201	0.219632	0.301815	0.301815	0.715313	0.0060338	0.14E-03
	CPC	292.979	0.2201	0.218008	0.246791	0.246791	0.733168	−0.130610	0.43E-03
	SHDW	292.979	0.2200	0.223534	0.239211	0.239211	0.741062	−0.148043	0.95E-03
	SPIN	292.979	0.2203	0.219788	0.138904	0.138904	0.405680	0.585348	0.27E-03
1.05	BIN	295.470	0.2200	0.216314	0.303688	0.303688	0.711680	0.0050144	0.98E-04
	CPC	295.539	0.2100	0.207452	0.277308	0.277308	0.720437	−0.073438	0.51E-03
	SHDW	295.539	0.2100	0.232388	0.237922	0.237922	0.744621	−0.160574	0.13E-02
	SPIN	295.470	0.2182	0.216473	0.140612	0.140612	0.403228	0.0602617	0.27E-03
1.15	BIN	301.327	0.2106	0.208248	0.309228	0.309228	0.694913	0.0244357	0.41E-03
	CPC	301.626	0.1800	0.186959	0.283381	0.283381	0.724683	−0.145573	0.64E-03
	SHDW	301.626	0.2570	0.250631	0.213515	0.213515	0.740152	−0.124530	0.41E-03
	SPIN	301.327	0.2106	0.208629	0.145389	0.145389	0.393367	0.0735758	0.31E-03
1.30	BIN	308.885	0.1994	0.198690	0.313282	0.313282	0.686420	0.0156524	0.20E-03
	CPC	310.119	0.1600	0.159984	0.325545	0.325545	0.698045	−0.112287	0.29E-03
	SHDW	310.119	0.2678	0.267974	0.196472	0.196472	0.728007	−0.099690	0.33E-03
	SPIN	308.885	0.1994	0.198823	0.149873	0.149873	0.388708	0.705170	0.23E-03
1.50	BIN	317.511	0.1860	0.187696	0.319475	0.319475	0.674091	0.102031	0.11E-03
	CPC	320.032	0.1400	0.133424	0.361751	0.361751	0.688941	−0.186053	0.11E-02
	SHDW	320.032	0.2729	0.280321	0.180506	0.180506	0.715549	−0.096547	0.24E-03
	SPIN	317.511	0.1860	0.187718	0.155539	0.155539	0.381119	0.0720636	0.10E-03
					$\langle r\rangle = 125$				
1.01	BIN	405.674	0.0821	0.0817586	0.388740	0.388740	0.470267	0.0530527	0.11E-03
	CPC	405.671	0.0825	0.0809932	0.374322	0.374322	0.473556	0.0118508	0.16E-03
	SHDW	405.664	0.0838	0.0834587	0.367208	0.367208	0.479764	−0.0047569	0.45E-03
	SPIN	405.674	0.0832	0.0817616	0.206312	0.206312	0.267830	0.0931012	0.12E-03
1.05	BIN	406.952	0.0820	0.0803534	0.388600	0.388600	0.466911	0.0500389	0.14E-03
	CPC	406.985	0.0773	0.0767843	0.383063	0.383063	0.468387	0.0102358	0.17E-03
	SHDW	406.985	0.0875	0.0872517	0.364996	0.364996	0.482525	0.0010258	0.17E-03
	SPIN	406.952	0.0800	0.0803039	0.207714	0.207714	0.265493	0.0940834	0.12E-03
1.15	BIN	409.874	0.0774	0.0770231	0.391561	0.391561	0.457668	0.0532519	0.92E-04
	CPC	410.105	0.0745	0.0679923	0.396395	0.396395	0.463669	−0.0404969	0.12E-02
	SHDW	410.105	0.0925	0.0951709	0.349345	0.349345	0.486639	0.0181239	0.10E-02
	SPIN	409.874	0.0770	0.0770066	0.209723	0.209723	0.260339	0.0959331	0.11E-03
1.30	BIN	413.652	0.728	0.0728143	0.393639	0.393639	0.446052	0.0529079	0.97E-04
	CPC	414.342	0.0600	0.0562399	0.441398	0.441398	0.444438	−0.056081	0.31E-03
	SHDW	414.342	0.0968	0.102827	0.324445	0.324445	0.495663	−0.0371434	0.36E-03
	SPIN	413.652	0.0728	0.0727872	0.210996	0.210996	0.253674	0.0967061	0.99E-04
1.50	BIN	417.839	0.0695	0.0681221	0.397167	0.397167	0.432536	0.0544505	0.69E-04
	CPC	419.191	0.0500	0.0460946	0.454923	0.454923	0.416889	−0.0281722	0.20E-02
	SHDW	419.191	0.1024	0.107228	0.315779	0.315779	0.488858	−0.0296032	0.20E-02
	SPIN	417.839	0.0695	0.0680961	0.214484	0.214484	0.246014	0.0983306	0.86E-04
					$\langle r\rangle = 1250$				
1.01	BIN	455.118	0.0280	0.0273821	0.427641	0.427641	0.280774	0.0581572	0.21E-04
	CPC	455.116	0.0275	0.0271334	0.421771	0.421771	0.280436	0.0583445	0.62E-04
	SHDW	455.116	0.0285	0.0279159	0.419939	0.419939	0.282775	0.0560498	0.62E-04
	SPIN	455.118	0.0280	0.0273979	0.234080	0.234080	0.157349	0.134999	0.83E-04
1.05	BIN	455.598	0.0270	0.0268677	0.428074	0.428074	0.277413	0.0688570	0.27E-04
	CPC	455.610	0.0265	0.0255861	0.429863	0.429863	0.274223	0.0816814	0.84E-04
	SHDW	455.610	0.0290	0.0294385	0.408694	0.408694	0.282955	0.0904725	0.11E-03
	SPIN	455.598	0.0270	0.0268728	0.234838	0.234838	0.157052	0.119928	0.54E-04
1.10	BIN	456.688	0.0255	0.0256909	0.431563	0.431034	0.271549	0.0677599	0.28E-04
	CPC	456.783	0.0220	0.0223129	0.451275	0.451275	0.266868	0.0591597	0.45E-04
	SHDW	456.783	0.0325	0.0321458	0.406889	0.406889	0.288640	0.0982202	0.67E-04
	SPIN	456.688	0.0255	0.0256997	0.241050	0.213270	0.153051	0.148427	0.60E-04
1.30	BIN	458.087	0.0240	0.0242041	0.431632	0.431632	0.263683	0.0691450	−23E-04
	CPC	458.365	0.0180	0.0184557	0.478514	0.478514	0.253491	0.0436774	0.26E-04
	SHDW	458.365	0.0353	0.0347401	0.389630	0.389517	0.288719	0.104764	0.84E-04
	SPIN	458.087	0.0240	0.0241900	0.239389	0.239389	0.146530	0.152518	0.95E-04
1.50	BIN	459.622	0.0225	0.0225903	0.428056	0.428056	0.252136	0.105652	0.71E-04
	CPC	460.157	0.0150	0.0147380	0.505073	0.505073	0.236102	0.0420337	0.30E-04
	SHDW	460.157	0.0361	0.0364149	0.364670	0.364670	0.283929	0.0886810	0.75E-04
	SPIN	459.622	0.0225	0.0225671	0.239288	0.239288	0.142079	0.148215	0.79E-04

[a] Since $\alpha = 0$, $B_1 = B_2$.

cal results are reported in Table 10. Figure 12a shows the ratio $T_{CP,max}/T_c$, and Figure 12b $\psi_{CP,max}/\psi_c$, both *vs* ϱ_m for polymer solutes of different average segment number ($\langle r\rangle_n$ = 12.5, 125, and 1250). Our immediate interest is in the neighborhood of $\langle r\rangle_w \approx 125$ and $\varrho_m \approx 1.05$. From Table 10 and/or Figure 12a we conclude that use of BIN to interpret CP data at $\varrho_m \approx 1.05$ (*i.e.* erroneously interpreting the observed maximum as (T_c,ψ_c)) gives an overestimate of ≈0.02% for T_c, and from Figure 12b, an underestimate of ≈4% for ψ_c, assuming the correct value for $\langle 1/r\rangle_w$ is employed. The BIN-based estimate for χ is thus displaced from the more nearly correct polydisperse value by ≈0.02%. Furthermore, that estimate will contain an additional imprecision of $(100/\langle r\rangle_w{}^*\delta\langle r\rangle_w/\langle r\rangle_w)\%$ where $\delta\langle r\rangle_w$ is the uncertainty in the weight average segment number. If, on the other hand, data analysis takes polydispersity into account, the investigator will be most interested in the imprecision which results from uncertainty in ϱ_m (assuming $W(r)$ is of the correct form). At $\langle r\rangle_w = 125$, Figure 12a

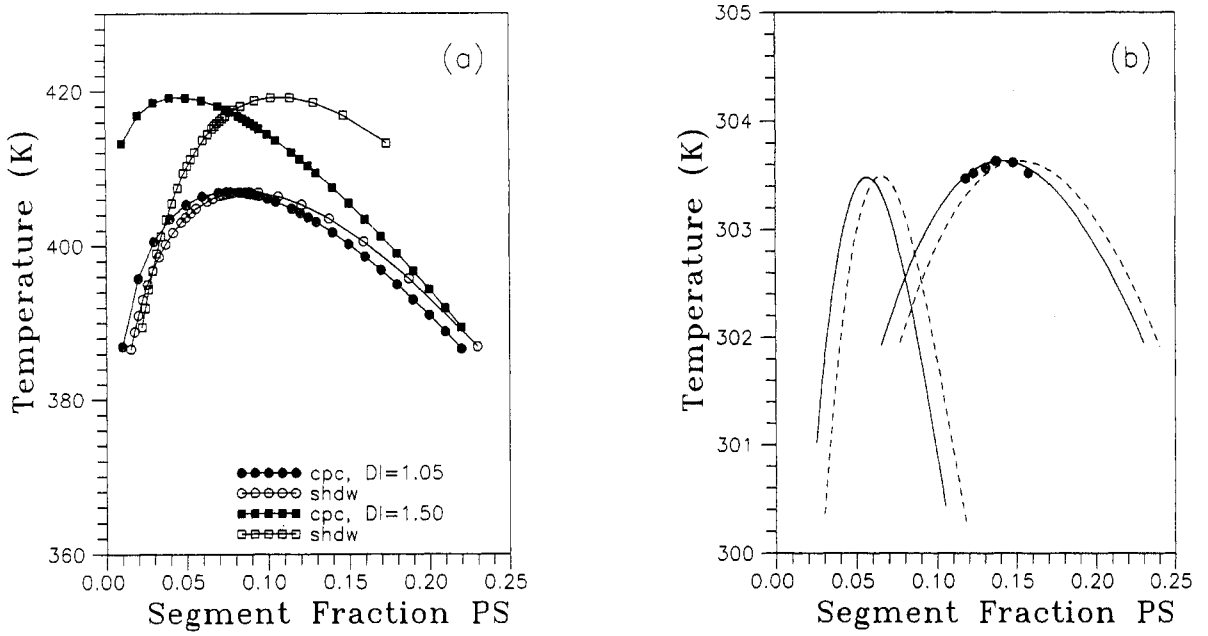

Figure 11. The effects of polydispersity and higher order terms in the concentration expansion on UCS demixing curves. (a) The effect of polydispersity on CP and SHDW curves. The zero order FH description. Upper $\varrho_m = 1.5$, lower $\varrho_m = 1.05$. For both sets $\chi_{0,0} = 2000$ J·mol^{-1} and all other χ's in eqs 25–27 = 0. Also $\langle r\rangle = 125$, and $MW_{solvent} = 58$ g·mol^{-1}. Dispersity index (DI) = $\varrho_m = M_w/M_n$. CP curves are through solid points, and SHDW curves through open points. (b) The effect of higher terms in the concentration expansion on CP and SHDW. For all curves $\langle r\rangle = 240$, $\varrho_m = 1.06$, and $MW_{solvent} = 84.2$ g·mol^{-1}. Left curves $\chi_{0,0} = 1425$ J·mol^{-1} and all other parameters in eq 28 zero; right-hand curves $\chi_{0,0} = 2039.51$ and $\chi_{1,0} = -248.38$ J·mol^{-1}, all other parameters zero; the heavy points show experimental data for MCP/PS.

demonstrates that an uncertainty of ±0.01 in ϱ_m (at $\varrho_m = 1.05 \pm 0.01$) is equivalent to one in T_c of ≈0.01% and in ψ_c of ≈0.005%. The resulting uncertainty in χ_0 is $\approx(0.03 + (100/\langle r\rangle_w)*\delta\langle r\rangle_w/\langle r\rangle_w)\%$.

Not too close to (T_c,ψ_c) fractionation effects become important. Figures 12c and 12d, 12e and 12f, and 12g and 12h show plots of T_{CP}/T_{BIN} and T_{SHDW}/T_{BIN} *vs* segment fraction, ψ, at selected values of ϱ_m for $\langle r\rangle_{n,CP} = 12.5$, 125, and 1250, respectively. In each case the intersection of the various curves defines the critical point. As $\langle r\rangle$ increases the curves sharpen markedly and critical points shift to lower and lower concentration (from $\psi \approx 0.2$ at $\langle r\rangle = 12.5$ to $\psi \approx 0.02$ at $\langle r\rangle = 1250$). Figures 12i through 12k show T_{CP}/T_{BIN}, T_{SHDW}/T_{BIN}, and ψ_{CP}/ψ_{BIN} plotted *vs* T_{BIN} for $\langle r\rangle = 125$ at various values of ϱ_m. Finally, Figure 12 shows $\langle r_{SHDW}\rangle$ *vs* ψ_{SHDW} for $\langle r\rangle = 125$ at various ϱ_m. In each case the differences between cloud or shadow curve and the monodisperse BIN approximation become appreciable as ϱ_m increases above a few percent or so. They cannot be ignored in accurate work.

Other projections of the results of the calculations reported in Table 10 are possible, but those shown in Figure 12 suffice to illustrate the principal features of interest. For samples with $1.0 \le \varrho_m \le 1.1$, say $\varrho_m = 1.05$, the BIN approximation gives errors on the order of a few tenths Kelvin, and a few thousanths to a hundreth or so segment fraction units, and a corresponding error for χ as determined from the phase diagram (*vide supra*). If, on the other hand, one elects a polydisperse treatment the systematic errors described above are replaced with uncertainties which are factors of $\approx\delta\varrho_m/(\varrho_m - 1)$ smaller ($\delta\varrho_m$ is the uncertainty in ϱ_m). We close this section with the *caveat* that these conclusions are strictly correct only for SF polymers. However it seems well established that *W(r)* for the SF distribution is representative of *W(r)* for many polymer samples and it is reasonable to conclude that the error analysis discussed above is also a reasonable approximation. We are currently engaged in extending calculations to other MW distributions, including distributions of arbitrary shape.

To sum up, in a practical sense these calculations demonstrate that experiments using samples of low polydispersity, say 1.05 or less, are in fact very good systems to use for testing the predictions of theories and simulations carried out in the monodisperse (BIN) approximation. By that we mean the difference between calculations in the polydisperse and BIN approximations will be order of magnitude comparable to the expected experimental error. However for higher polydispersity, say $\varrho_m \ge 1.1$, monodisperse calculations become inadequate to that point of being seriously misleading.

5.3b. Extended Form for G^{ex}. The experimental data for PS in acetone, methylcyclpentane, and propionitrile[46] solutions show upper (UCS) and lower (LCS) branches and hypercritical points which depend on P, $\langle r\rangle$, ϱ_m, ψ, and y_D and z_D. If the statistical model leading to eqs 13 and 14 is accurate, one expects all of the "*r*" dependence to be accounted for in the standard state and ideal mixing terms. If, on the other hand, the model is not exact, or if the parameters which define the ideal contribution (principally r_A and $\langle r_B\rangle$) are inappropriately chosen, some residual "*r*" dependence will remain, and for the want of another home will become incorporated in the excess free energy term. In that context we conclude that G^{ex} may be a function of as many as six variables, $G^{ex} = G^{ex}(T,P,\psi,r,y_D,z_D)$.

It is convenient to separate the concentration dependence of G^E by introducing a set of parameters, $\chi_i = \chi_i(T,P,r,y_D,z_D)$, $\chi_i = \chi_i/(T)$. Following many others we write

$$G^{ex}/(R) = \psi(1-\psi)(\chi_0 + \chi_1(1-2\psi) + \chi_2(1-2\psi)^2 + \ldots) \quad (25)$$

It is understood the χ's may be functions of T, P, r, y_D,

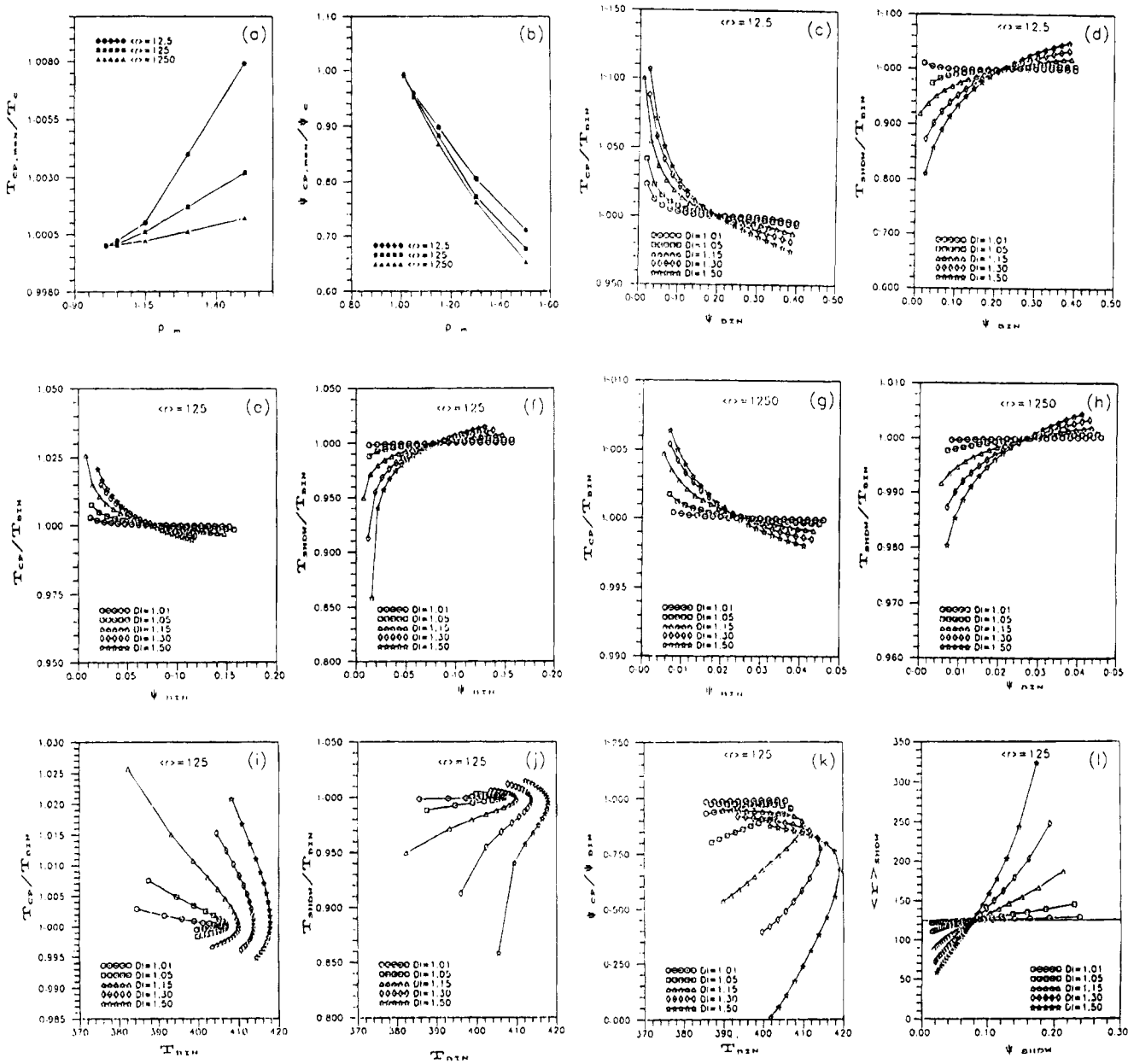

Figure 12. Calculated fractionations and related effects for UCS demixing in Schulz–Flory solutions according to a zero order FH description which includes the effects of polydispersity. Comparisons with the monodisperse approximation. The plots in this figure refer to the calculations reported in Table 10. (a) $T_{CP,max}/T_c$ *vs* ϱ_m at $\langle r\rangle$ = 12.5, 125, and 1250. (b) $\psi_{CP,max}/\psi_{CP,c}$ *vs* ϱ_m at $\langle r\rangle$ = 12.5, 125, and 1250. (c) T_{CP}/T_{BIN} *vs* ψ_{BIN} for various ϱ_m at $\langle r\rangle$ = 12.5. (d) T_{SHDW}/T_{BIN} *vs* ψ_{BIN} for various ϱ_m at $\langle r\rangle$ = 12.5. (e) T_{CP}/T_{BIN} *vs* ψ_{BIN} for various ϱ_m at $\langle r\rangle$ = 125. (f) T_{SHDW}/T_{BIN} *vs* ψ_{BIN} for various ϱ_m at $\langle r\rangle$ = 125. (g) T_{CP}/T_{BIN} *vs* ψ_{BIN} for various ϱ_m at $\langle r\rangle$ = 1250. (h) T_{SHDW}/T_{BIN} *vs* ψ_{BIN} for various ϱ_m at $\langle r\rangle$ = 1250. (i) T_{CP}/T_{BIN} *vs* T_{BIN} for various ϱ_m at $\langle r\rangle$ = 125. (j) T_{SHDW}/T_{BIN} *vs* T_{BIN} for various ϱ_m at $\langle r\rangle$ = 125. (k) ψ_{CP}/ψ_{BIN} *vs* T_{BIN} for various ϱ_m at $\langle r\rangle$ = 125. (l) $\langle r\rangle_{SHDW}$ *vs* ψ_{SHDW} for various ϱ_m at $\langle r\rangle$ = 125. In the figures ϱ_m is denoted as the dispersity index (DI). Also $\chi_{0,0}$ = 2000 J·mol^{-1} and all other χ parameters are zero (see eqs 25 and 27).

and z_D, but not ψ. For acetone solutions double extrema on CP curves are observed in the hypercritical region and one is unable to rationalize that observation with fewer than three χ_i parameters. Solving for activity coefficients under the constraints imposed by the Gibbs–Duhem relation one obtains,

$$RT\ln(f_A) = a_1\psi^2 + b_1\psi^3 + c_1\psi^4$$

$$RT\ln(f_B) = a_2(1-\psi)^2 + b_2(1-\psi)^3 + c_2(1-\psi)^4 \tag{26}$$

where $a_1 = \chi_0 + 3\chi_1 + 5\chi_2$, $a_2 = \chi_0 - 3\chi_1 + 5\chi_2$, $b_1 = -4\chi_1 - 16\chi_2$, $b_2 = 4\chi_1 - 16\chi_2$, and $c_1 = c_2 = 12\chi_2$. Analogous expressions are available should eq 25 be employed to order 3 or higher.[47]

For the other variables it is useful to expand the χ_i about an arbitrary origin denoted "*". A convenient choice, for example, might be ($P^* = 0$, $T^* = T_{hyp}$, $y_D^* = 0$, $z_D^* = 0$). If both UCS and LCS branches are observed in any of the $(T,\psi)_{P,y_D,z_D,\varrho_m}$, $(P,\psi)_{T,y_D,z_D,\varrho_m}$, $(y_D,\psi)_{T,P,z_D,\varrho_m}$, *etc.* projections, the dependence of χ must be at least quadratic in the relevant coordinate conjugate to ψ.[48] For PS/acetone, PS/methylcyclopentane, and PS/propionitrile solutions we have observed both UCS and LCS branches only in the (T,ψ) plane and conclude that quadratic and higher terms *are not necessarily required* in the (P,ψ), (y_D,ψ), (z_D,ψ), (r^{-1},ψ), *etc.* projections. (The possibility of observing more than one demixing branch in any of these other projections is intriguing and worth further investigation.) For that reason we elected

Table 11. Synopsis of Range and Number of Data Points Considered in the Analysis of This Paper

SYS	polym code[a]	MW	ϱ_m	no. conc	y_D	z_D	temp range/K	pressure range/MPa
				System: Polystyrene–Acetone				
1	B	8000	1.09	1	0	0	252.83–253.77	0.07–1.25
2	B	8000		1	0.564	0	270.67–271.42	0.24–1.07
3	B	8000		1	0.670	0	274.54–275.78	0.06–1.27
4	C	11687	1.03	1	0	0	273.75–274.91	0.41–1.72
5	D	13502	1.06	7	0	0	281.30–287.13	0.05–1.55
6	D	13502		9	1	0	328.09–384.97	0.26–2.77
7	D	13502		1	0.483	0	302.77–307.34	0.32–1.85
8	D	13502		1	0.719	0	313.76–319.15	0.38–1.95
9	D	13502		1	0.952	0	330.82–384.87	0.34–2.11
10	E	22091	1.03	10	0	0	321.19–378.35	0.26–2.00
11	H	10512	1.02	1	0	1	234.95–235.25	0.15–1.55
12	H	10512		1	1	1	266.69–268.78	0.47–2.61
13	I	26890	1.06	7	0	1	273.48–277.36	0.31–2.25
14	I	26890		13	1	1	274.58–278.61	0.35–2.23
				System: Polystyrene–Methylcyclopentane				
1	D	13502	1.06	1	0	0	291.30–291.78	0.45–2.00
2	E	22091	1.03	1	0	0	299.99–300.75	0.51–2.59
3	F	25000	1.06	7	0	0	302.53–303.51	0.19–2.90
4	F	25000		1	0.943	0	308.58–309.76	0.59–2.88
5	G	106280	1.06	1	0	0	325.19–327.01	0.55–2.45
6	G	106280		1	0.943	0	336.23–338.45	0.64–2.13
7	A	4136	1.06	1	0	0	259.49–259.62	1.30–3.70
8	I	26890	1.06	1	0	1	302.48–303.39	0.23–2.52
9	I	26890		1	0.943	1	307.74–308.67	0.42–2.25

[a] See Table 1.

slightly different forms for the temperature dependence as compared to those for the other variables, writing

$$\chi_i(T,P,r,y_D,z_D) = [\chi_{i,0} + \chi_{i,1;T}(T) + \chi_{i,2;T}(T^2) + ... + \chi_{i,1;P}(P) + \chi_{i,2;P}(P^2) + ... + \chi_{i,1;r}(r^{-1}) + \chi_{i,2;r}(r^{-1})^2 + ... + \chi_{i,1;y_D}(y_D) + \chi_{i,2;y_D}(y_D^2) + ... + \chi_{i,1;z_D}(z_D) + ... \quad (27)$$

6. Comparison with Experiment

We have employed eqs 26 and 27 to rationalize demixing data for PS/acetone and PS/methylcyclopentane solutions following the scheme outlined above, taking full account of polydispersity in the approximation of Schultz–Flory distributions and using PHASEEQ^r for numerical analysis. The range of concentrations, temperatures, pressures, and isotope labels are reviewed in Table 11. Our initial experience with PHASEEQ^r in the hypercritical region was that convergence is highly sensitive to the choice of parameters. We therefore elected to employ the simplest possible initial set (*i.e.* choosing the fewest possible higher order terms), after some trial and error arriving at a form which we have found to be the simplest to reasonably describe the available data

$$G^{ex}/[(R)\psi(1-\psi)] = [\chi_{0,0} + \chi_{0,1;T}(T) + \chi_{0,2;T}(T^2) + \{\chi_{0,1;P} + \chi_{0,1;P,r}{}^*(1/\langle r\rangle)\}{}^*(P) + \{\chi_{0,1;r0} + \chi_{0,1;r1}(\langle r\rangle) + \chi_{0,1;r2}(\langle r\rangle^2)(\langle r\rangle^{-1}) + \chi_{0,1;y_D}(y_D) + \chi_{0,1;z_D}(z_D) + [\chi_{1,0} + \chi_{1,1;T}(T) + \chi_{1,2;T}(T^2)](1-2\psi) + \chi_{2,0}(1-2\psi)^2 \quad (28)$$

In arriving at eq 28 we have assumed that the P, r, y_D, and z_D dependence of G^E can be placed in the (0,1)th order term. The existence of both an upper and a lower demixing branch demands temperature dependence to be at least quadratic. We are aware that refinements in experimental data and/or theoretical interpretation may later require the inclusion of higher order terms for the other variables.

To begin with it is important to consider the effect of concentration broadening on CP, SHDW, SP, and BIN (see Figure 11b). Although the presence of a double maximum in CP for PS/acetone in the hypercritical region implies the necessity of terms through order $\chi_{2,0}$ in that part of the phase diagram, the Cp curves smooth as one moves away from T_{hyp}, and over most of the phase diagram the double minimum is not observed. In the preliminary calculations, therefore, we considered concentration broadening only through order $\chi_{1,0}$ so that we could simplify the interpretation as much as possible and minimize the number of arbitrarily selected parameters. It is clear from Figure 11b that a proper description of the observed concentration dependence of CP must include at least one term beyond zero order.

The parameters chosen to describe temperature dependence for G^E ($\chi_{0,1;T}$, $\chi_{0,2;T}$, and $\chi_{1,1;T}$, $\chi_{1,2;T}$) were obtianed by fitting SOLVENTh/PSh (SOLVENTh = ACh or MCPh) UCS and LCS CP data for a selected value of $\langle r\rangle$. As shown in Figure 13a for the ACh/PSh case this forces agreement in the (T_c,$1/\langle r\rangle$) plane, but at the chosen value of $1/\langle r\rangle$ only. The mismatch of calculation and experiment at other values of $1/\langle r\rangle$ demonstrates the need for an "r" dependence in the expression for G^E. More exactly, one can say the observed $1/r$ dependence of CP is incorrectly described by the statistical model leading to the ideal mixing term in the first part of eq 22. We have elected to correct for the deficiency by including an $\langle r\rangle$ dependent term in the expression for G^E. The expansion is empirical (eq 28), we found it necessary to include terms through order r^2 to properly describe the observed CP data. Figure 13a compares calculated (solid line) and experimental UCS and LCS critical temperatures (points) for PS/ACh solutions, and compares the result with calculated values in the absence of the "$1/\langle r\rangle$" correction, *i.e.* for $\chi_{0,1;r} = 0$ (dashed line). A comparison with the scaling fit to the experimental data (Table 8) is also included (dotted line).

Figure 13b compares calculated and experimental projections in the (T_c,$1/\langle r\rangle$) plane for polystyrene–acetone systems, comparing the effects of isotopic label and pressure. The reference solution, PSh/ACh (P = 0) is compared with the labeled solutions PSh/ACd, PSd/

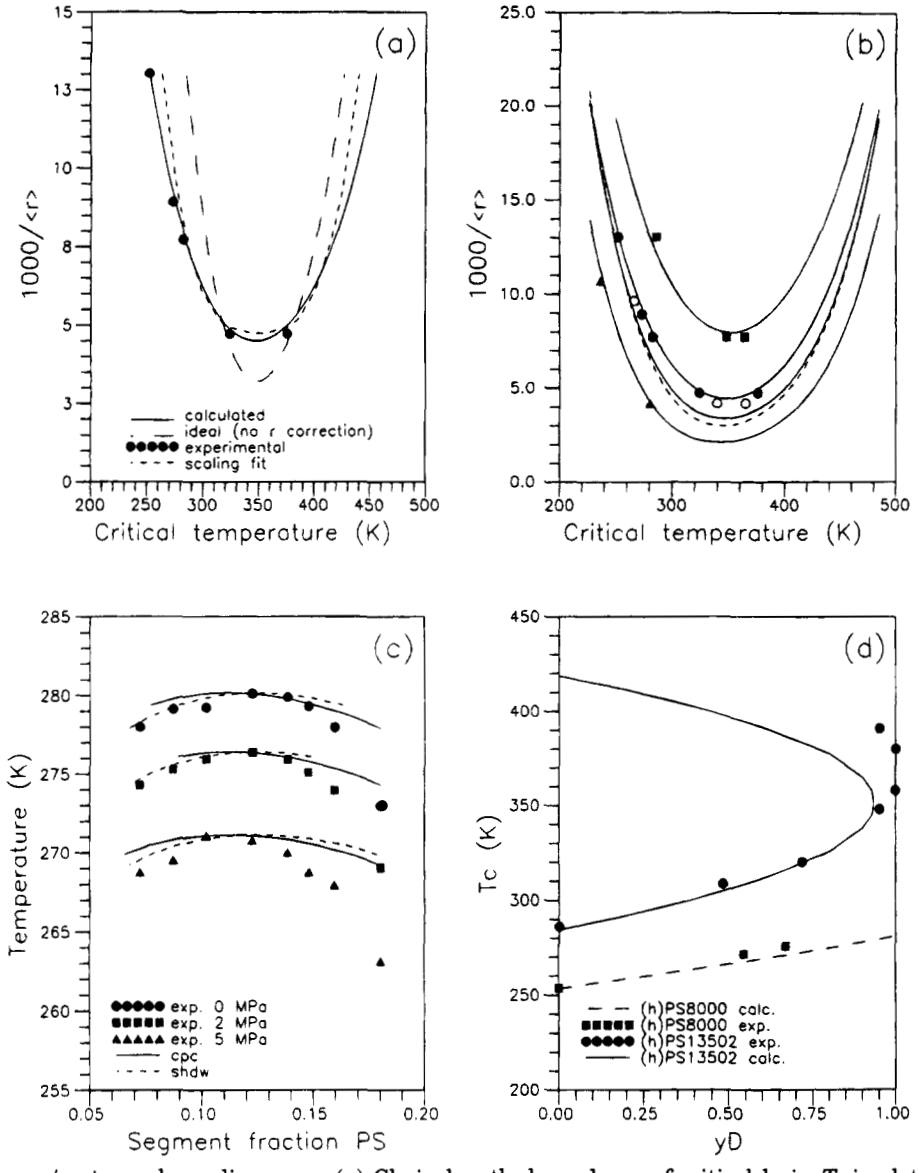

Figure 13. Polystyrene/acetone phase diagrams. (a) Chain length dependence of critical loci. T_c is plotted atainst $1/\langle r\rangle$ for PS/AC data. The points are experimental. The dashed curve is a fit of eq 27 to the data for $\langle r\rangle = 130$, but assuming no "r" dependence in the excess free energy term. The solid line is then obtianed by using the "r" dependent G^{ex} given by the parameters in Table 12 (PS/AC). The dotted curve is the scaling fit from Table 8. (b) Chain length dependence of critical loci for variously substituted h/d polystyrenes and acetones. The curves are calculated from the parameters of Table 12 (PS/AC). Reading down at the minima: PS(h)/AC(d), P/MPa = 0 (expt = solid squares, 2 MPa); PS(h)/AC(h), P/MPa = 0 (expt = solid dots, 2 MPa); PS(d)/AC(d), P/MPa = 2 (expt = open dots, 0 MPa); PS(h)/AC(h), P/MPa = 5 (dotted line); PS(d)/AC(h), P/MPa = 0 (expt = solid triangles). (c) Calculated CP and SHDW data for PS(d)/AC(h) ($\langle r\rangle = 260$, $\varrho_m = 1.06$) in the (T_c,ψ) plane compared with experiment at several pressures. The lines are calculated from the parameters of Table 3 (PS/AC). (d) Calculated CP data for PS/AC in the (T_c,y_D) plane compared with experiment at several values for $\langle r\rangle$ (inner curve [solid line, $\langle r\rangle = 130$, $\varrho_m = 1.06$; outer curve [dashed line], $\langle r\rangle = 77$, $\varrho_m = 1.06$. The lines are calculated from the parameters of Table 12.

ACh, and PSd/ACd, all at nominal $P = 0$, and with PSh/ACh at elevated pressure ($P = 5$ MPa). The parameters are reported in Table 12; agreement between experiment and calculation is satisfactory. Both the magnitude and the ordering of the IE's are nicely represented, as is the "r" dependence. Note that the PSd/ACd effect is calculated from the independently determined parameters $\chi_{0,1;y_D}$ and $\chi_{0,1;z_D}$ in good agreement with experiment. Figure 13c compares calculated CP and SHDW curves in the (T,ψ) projection for PSd/AC ($z_D = 1$) at several pressures for $\langle r\rangle = 241$, $\varrho_m = 1.06$ with experiment. The parameters used for the calculation are those from Table 12, and except for $\chi_{0,1;y_D}$, were chosen to fit PSh/ACh data. The excellent agreement between calculated and experimental T_c's as a function of pressure is therefore gratifying, even though the agreement decays as one moves away from (ψ_c,T_c) toward higher or lower concentration. For this particular sample $\langle r\rangle$ is nearly at its hypercritical value and the phase diagram in the (T,ψ) plane is extremely sensitive to the choice of parameters. Better agreement for the ψ dependence is expected at lower values of $\langle r\rangle$ (*i.e.* further removed from $\langle r\rangle_{hcp}$). Figure 13d compares solvent isotope effects in the (y_D,T_c) projection for several values of $\langle r\rangle$, one close to the hypercritical $\langle r\rangle$, the other well removed. Comparison with experimental data is remarkably good. Recall that just one parameter is employed to describe the solvent isotope effect (y_D dependence) over the entire concentration, segment number, temperature, and pressure range. Although not shown, calculated demixing plots in the (T_c,P), and (T_c,z_D) projections are analogous to Figure 13d and also show good agreement with experiment.

Table 12. Continuous Thermodynamic Interpretation of Polystyrene/Solvent Liquid–Liquid Demixing Data: Mean-Field Parameters of Fit to Eq 28) for Acetone–Polystyrene and Acetone–Methylcyclopentane Solutions[a]

param	PS/AC	PS/MCP
$\chi_{0,0}$	2398.44	2506.79
$\chi_{0,1;T}$	−7.36154	−7.31916
$\chi_{0,2;T}$	0.0197205	0.0183679
$\chi_{0,1;P}$	−13.396	−2.20159
$\chi_{0,1;P,r}$	721.99	79.70
$\chi_{0,1;r0}$	−10640.9	
$\chi_{0,1;r1}$	8.6552898	
$\chi_{0,1;r2}$	0.22278615	
$\chi_{0,1;y_D}$	95.	18
$\chi_{0,1;z_D}$	−102.51	−3
$\chi_{1,0}$	−2.91007	11.1949
$\chi_{1,1;T}$	−0.672534	−0.76503
$\chi_{1,2;T}$		
$\chi_{2,0}$		

[a] $G^e_x[[(R)\psi(1-\psi)] = [\chi_{0,0} + \chi_{0,1;T}(T) + \chi_{0,2;T}(T^2) + \{\chi_{0,1;P} + \chi_{0,1;P,r}{}^*(1/\langle r\rangle)\}{}^*(P) + \{\chi_{0,1;r0} + \chi_{0,1;r1}(\langle r\rangle) + \chi_{0,1;r2}(\langle r\rangle^2)\}(\langle r\rangle^{-1}) + \chi_{0,1;y_D}(y_D) + \chi_{0,1;z_D}(z_D) + [\chi_{1,0} + \chi_{1,1;T}(T) + \chi_{1,2;T}(T^2)](1-2\psi) + \chi_{2,0}(1-2\psi)^2$.

The calculations for the PS/MCP solutions were carried out like those described for PS/AC, above. Parameters are reported in Table 12. Figure 14 compares calculated and experimental CP data in the $(T_c,1/\langle r\rangle)$ plane. MCP is a much better solvent than is AC and the homogeneous region persists to infinite $\langle r\rangle$, defining upper and lower Θ points. The present demixing experiments were made along the UCS (lower temperature) branch only and primarily define the parameters describing the temperature dependence (Table 11). The data defining the LCS (upper branch) are from other laboratories,[34] and those individual data points, although not shown on the figure, are well represented by the scaling fit (shown as the dotted line). The $\langle r\rangle$ dependence of G^E is much smaller in PS/MCP than it is for PS/AC. To present precision it can be taken as zero (compare Figures 13a and 14). (The outlier point close to the bottom of the diagram refers to a very high molecular weight sample with ϱ_m poorly characterized. It was not included in the least squaring.) In the interests of saving space we have not presented plots which compare calculated and observed CP data for PS/MCP solutions in the (T,ψ) and (T_c,y_D) projections, (*i.e.* to compare with Figures 13c and 13d), but the agreements between calculation and experiment are at least as good as those for PS/AC.

The observation that the $\langle r\rangle$ dependence of MCP/PS solutions is adequately described by the ideal FH mixing term, but that for AC/PS solutions it requires a significant contribution from an $\langle r\rangle$ dependent G^E is noteworthy. The AC/PS systems display a hypercritical point which severely constrains the range of possible fitting parameters (*i.e.* constrains the calculated line in the $(T,1/\langle r\rangle)$ projection (Figure 13a) to a specific minimum, $(T,1/\langle r\rangle)_{hyp}$). MCP/PS, on the other hand, shows upper and lower Θ points, but no hypercritical minimum is observed, and the constraints on the fitting parameters are not as severe. In other words the AC/PS data afford a stricter test of the theory, which in its most straightforward form should account for the $1/\langle r\rangle$ dependence of the phase transition in the ideal part of the expression for the free energy. That does not work for AC solutions. The point of interest is that it likely does not work for MCP solutions either, the apparent improvement in the quality of fit is probably an artifact consequent to relaxing the hypercritical constraints.

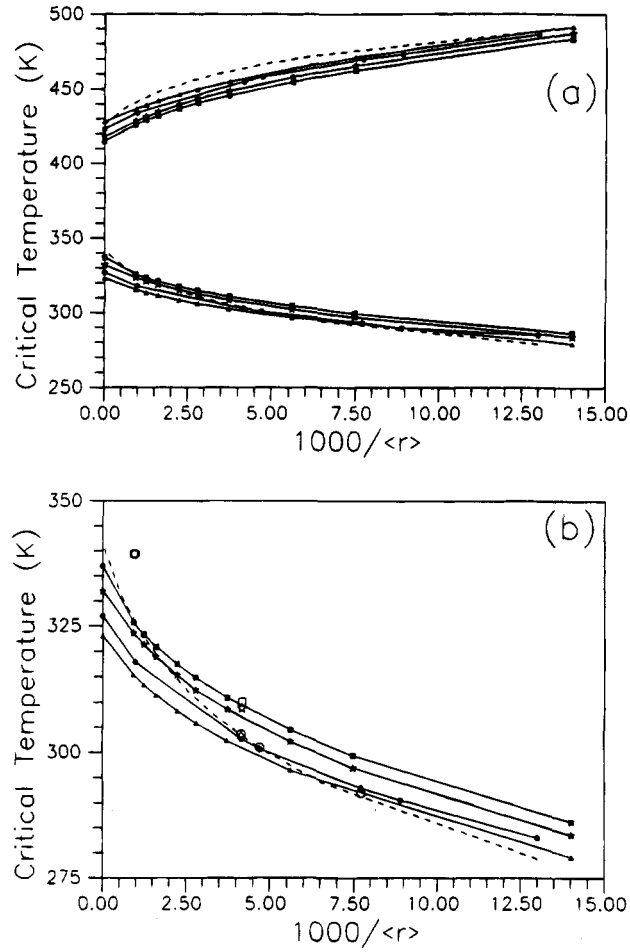

Figure 14. Polystyrene/methylcyclopentane phase diagrams. (a) Chain length dependence. T_c is plotted against $1/\langle r\rangle$ for PS/MCP data. The curves are calculated from the parameters of Table 12 (PS/MCP) except for the scaling fit, which is from Table 8. (b) Chain length dependence. Enlargement of the low temperature branch shown in Figure 14a. In both (a) and (b) the points connected with solid lines represent calculations, the open symbols show experimental data: squares = MCPd/PSh; stars = MCPd/PSd; circles = MCPh/PSh; triangles = MCPh/PSd. The dashed line is the scaling fit to MCPh/PSh.

Thus the theory is more strictly tested by systems which display both UCS and LCS branches than by ones displaying only one branch, and it is even more strictly tested by systems with UCS and LCS branches which join at a hypercritical point than it is by ones which do not so join. Presumably, a more nearly correct theory will be able to treat the $1/\langle r\rangle$ dependence of the precipitation phenomena as an integral part of the statistical analysis (*i.e.* independent of solvent).

Figure 15 reports on the effect of adding a quadratic term to the concentration dependence of the excess free energy. It shows the present model can yield phase diagrams with double extrema for both UCS and LCS branches (only the UCS branch is shown) and, in the hypercritical region, can predict isolated one-phase regions in the developing hourglass configuration as observed in PS/AC solutions. Rewriting eq 28, we introduced the second order term, $(\chi_{2,0}(1-2\psi)^2$, using eq 21 and its next higher concentration derivative to fix the ratios χ_{20}/χ_{10} and χ_{10}/χ_0 from the spinodal

$$G^{ex}/[(R)\psi(1-\psi)] = \chi_0(T,P,r,y_D,z_D) + \chi_{1,0}(1-2\psi) + \chi_{2,0}(1-2\psi)^2 \quad (29)$$

constraints. We can perturb the result by adding in the

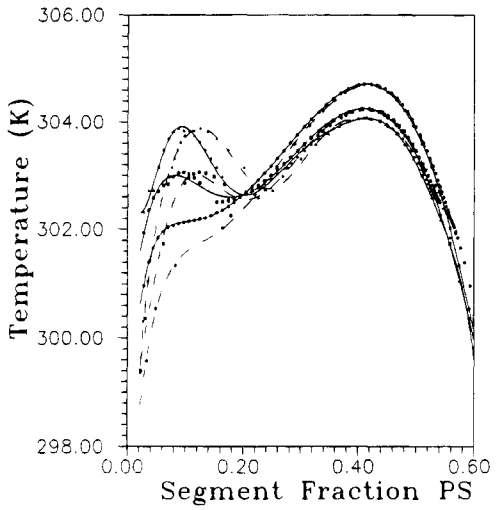

Figure 15. The effect of higher order terms on concentration broadening for a PSh/ACh solution, prediction of double maxima in cloud and shadow curves: $\langle r\rangle = 153.6$, $\varrho_m = 1.06$, $y_D = 0$, $z_D = 0$. Calculated CP and SHDW curves are shown for three sets of parameters. For these calculations G^{ex} is given by eq 29:

	χ_0	$\chi_{1,0}$	$\chi_{2,0}$	
●	2708.29	−733.04	181.88	(CP)
■	2708.29	−733.04	185.88	(CP)
▲	2708.29	−733.04	187.35	(CP)

In each case SHDW is shown as the dashed line.

pressure dependence, $\chi_{0,1;P}(P)$, to induce a UCS/LCS → "hourglass" transition. The equilibrium conditions are extremely sensitive to the choice of parameters which are in delicate balance (see caption, Figure 15). The large separation of CP and SHDW near the first maximum is especially interesting (ϱ_m is a modest 1.06). The calculated diagrams shown in Figure 15 do not show quantitative agreement with the very complicated hypercritically enhanced details observed in the (T,ψ) and (T,y_D) CP projections for PS/AC in the hypercritical region. Still, there is every indication that the model can be adjusted to more nearly reproduce those complications.

We conclude that the present model is useful. It is capable of representing the demixing properties of polydisperse polymer solutions with a limited number of parameters. Although we plan to develop algorithms to generate least-squares fits of experimental data with the above formalism, we have not yet done so. Therefore, the parameters reported in Table 12 are not optimized. Even so, the obvious qualitatively correct agreement between calculated and experimental CP's establishes the present treatment as reasonable. Moreover that judgement extends to the pressure, solute and solvent isotope, and molecular weight dependences.

7. Hypercritical Conditions as Reference State

7a. Generalized Representations. With critical points and ψ dependences of demixing curves established by fitting to eqs 27 and 28 (or, less accurately, to BIN), it becomes useful to further summarize the data by considering plots of critical loci in the (T_c,P), $(T_c,1/\langle r\rangle_w)$, (T_c,y_D), or (T_c,z_D) planes. Such plots have been shown in Figure 13, but the same result can be obtained by considering the spinodal loci (eq 21), remembering at the critical point $\partial^3 G_{tot}/\partial\psi^3 = 0$, and

$$1/(1-\psi)^2 - 1/(\psi^2\langle r\rangle_w) + \partial^3(G^{ex}/RT)/\partial\psi^3 = 0 \qquad (30)$$

With G^{ex}/RT available from eq 25 it is a straightforward matter to determine the critical and hypercritical parameters by solving eqs 21 and 30 simultaneously. Were the excess free energies available in functional form one might calculate CP using

$$T_c = T_{hyp} + \int(dT_c/d\eta)_c\, d\eta \qquad (31)$$

Here η is a generalized coordinate representing P, y_D, z_D, $\langle 1/r\rangle$, *etc.* That calculation is not possible in a predictive sense for the solutions we have chosen to study. The necessary free energy data are not available. Rather we regard eqs 30 and 31 as empirical relations with parameters to be fixed by least squares analysis or other means.

7b. Scaling Fits. An economical scaling representation of the data along the critical line is possible. The scaling formalism employs expansions over reduced coordinates, $t^* = (T_{hcp} - T_c)/T_{hcp}$, $p^* = (P_{hcp} - P_c)/P_{hcp}$), etc. We expand about one or another hypercritical origin, say $(T_{hcp}, \langle 1/r\rangle_{hcp}, (P = 0, y_D = 0, z_D = 0))$. With proper definitions of the various order parameters the different expansions are analagous and lead to eq 32

$$|t^*| = A_k\eta_k{}^{*\beta} + B_k\eta_k{}^{*(\beta+1/2)} + (c_kA_k/T_{hcp})\eta_k{}^{*(\beta+1)} + (c_kB_k/T_{hcp})\eta_k{}^{*(\beta+1.5)} \pm (c_k/T_{hcp})\eta_k{}^* \quad (k = \langle 1/r\rangle, P, y_D, \text{or } z_D) \qquad (32)$$

where $t^* = (1 - T_c/T_{hcp}{}^0)$, $\eta_{\langle r\rangle}{}^* = [1 - ((\Lambda_{\langle r\rangle}{}^{-1} - MW^{-1})/(\Lambda_{\langle r\rangle}{}^{-1} - MW_{hcp}{}^{-1})^0)]$, $\eta_p{}^* = [1 - ((\Lambda_p - P)/(\Lambda_p - P_{hcp}{}^0))]$, $\eta_{y_D}{}^* = y_D{}^* = [1 - ((\Lambda_{y_D} - y_D)/(\Lambda_{y_D} - y_D{}^0))]$, and $\eta_{z_D}{}^* = z_D{}^* = [1 - ((\Lambda_{z_D} - z_D)/(\Lambda_{z_D} - Z_D{}^0))]$. The Λ parameters are order-defining quantities described below. The last term, $\pm(c_k/T_{hcp})\eta_k{}^*$, corrects for skewing in the (t^*,η^*) plane and is not always required. We obtained eq 32 starting from the observation that the mean value of the upper and lower critical temperature, $\langle T_c\rangle = (T_{c,ucs} + T_{c,lcs})/2$ is rectilinear. By defining a symmetric function, τ^*

$$\tau^* = |1 - T_c/\langle T_{hcp}\rangle| = |1 - T_c/\{T_{hcp} + c_k\eta_k{}^*\}| \qquad (33)$$

to be represented with a scaling expansion,

$$|\tau^*| = A\eta_k{}^{*\beta} + B\eta_k{}^{*(\beta+1/2)} + \ldots \qquad (34)$$

we obtain eq 32. If B_k is neglected eq 32 simplifies.

Examples of fits to eq 32 have been shown in Figures 8 and 9. The figures correlate large amounts of data by plotting critical loci in the (T,y_D) and $(T,\langle MW\rangle_n{}^{-1})$ planes. The lines are least squares fits to eq 32; the points are experimental. Figure 9a shows demixing data in the $(T,\langle MW\rangle_n{}^{-1})$ plane for different isotope labels (*i.e.* varying y_D or z_D) at a common pressure. We could have equally well have presented results at a series of isobars and a common isotopic label (*i.e.* holding y_D and z_D constant and varying pressure) and obtained an analogous family of scaling curves. Higher pressure corresponds to better solvent quality, that is to broader one-phase envelopes which extend to larger $\langle r\rangle_{hcp}$. $\langle r\rangle_{hcp;P}$ is the hypercritical segment number at the specified pressure P. It is defined as that number of segments for which $\lim(\partial T_c/\partial\langle r\rangle^{-1}) \to \infty$ as $P \to P_{hcp}$. We define $P_{hcp}{}^\infty$ as the pressure for which $\lim(\partial T_c/\partial\langle 1/r\rangle_w) \to \infty$ as $\langle 1/r\rangle_{w=\infty} \to 0$ (*i.e.* infinite polymer molecular weight). The upper and lower Flory Θ points coincide at $(T_{hcp}{}^\infty, P_{hcp}{}^\infty)$. For $P > P_{hcp}{}^\infty$ the $(\langle 1/r\rangle_w, T_c)$ envelope continues to broaden. For better solvents $\langle 1/r\rangle_{hcp}$ may

even move into the negative quadrant and no longer be physically accessible under equilibrium conditions. For an example compare Figures 9a and 9b. At $P = 0.1$ MPa $(T_{hcp}^{\infty},\langle 1/r_{hcp}\rangle)$ is comfortably in the (+, +) quadrant for acetone-*h/d* solvents, while for MCP (which is a somewhat better solvent), $(T_{hcp}^{\infty},\langle 1/r_{hcp}\rangle)_{P=0.1MPa}$ has moved to the (+, −) quadrant.

Least squares fits of the demixing data for PS in acetone and methylcyclopentane are reported in Tables 6–9. One term expansions suffice for acetone/PS where the range in η_{MW}^* is only one decade, but two terms are needed for MCP where the range is wider. Data in the $(T_c,\eta_{y_D}^*)$ plane extend across the entire range, $0 \le y_D \le 1$; it is noteworthy that eq 32 can be employed at all. No scaling fits are reported in the η_p^*(MCP), $\eta_{y_D}^*$(MCP), $\eta_{z_D}^*$(MCP), or $\eta_{z_D}^*$(acetone) coordinates because insufficient data exist to define the curvature in a meaningful fashion.

7c. Illustration: A Three-Dimensional Case. Successive application of eq 31 in each of the η_k dimensions generates a surface of critical points in a $k + 1$ dimensional hyperspace. It is instructive to discuss the simplest three-dimensional case ($k = 2$, $c_k = 0$, $B_k = 0$, $\beta = 1/2$). Choosing, for example, $z^* = t^*$, $(0 \le z^* \le 1)$, and $\eta_1 = x^*$ and $\eta_2 = y^*$ (thus x^* and y^* might correspond to reduced $\langle 1/r\rangle_n$ and pressure), one defines an elliptical paraboloid in (x^*, y^*, z^*) space. The major and minor axes are equal to A_x and A_y when $z^* = 1$ (Figure 16).

$$z^* = A_x^{-2}x^{*2} + A_y^{-2}y^{*2} \tag{35}$$

If scaling holds over the entire range $(0 \le [x^* \text{ or } y^*] \le 1)$, $A_x = A_y = 1$. More commonly scaling equations are only useful near the origin and $A_x \ne A_y \ne 1$. The dependence of x^* on z^* at specified values of y^* may be expressed

$$x^* = A_x(z^* - y^{*2}/A_y^{\,2})^{1/2} = A_x' z^{*\prime 1/2} \tag{36}$$

where A_x' is the amplitude factor as commonly written. $z^{*\prime}$ is a new reduced variable defined in the equation. The cross sections sketched in Figure 16 demonstrate the x^* and y^* dependences of the liquid–liquid critical loci to be projected on the (x^*, z^*) and (y^*, z^*) planes. z^* is restricted to the range $[(y^{*2}/A_y^{\,2}) \le z^{*\prime} \le 1]$. By multiplying and dividing by $(1 - y^{*2}/A_y^{\,2})^{1/2}$ each (x^*,z^*) cross section can be rescaled to the customary $[0 \le z^{*\prime} \le 1]$. Generalizing the exponent and adding higher order terms and a term to correct for skewing yields an analogue of eq 32. The leading term is

$$x^* = A_x'' z^{*\prime\prime\beta} \qquad A_x'' = A_x(1 - y^{*1/\beta}/A_y^{\,1/\beta})^{\beta}$$
$$z^{*\prime\prime} = (z^* - y^{*1/\beta}/A_y^{\,1/\beta})/(1 - y^{*1/\beta}/A_y^{\,1/\beta}) \tag{37}$$

The development shows that the parameters of the (x^*, z^*) scaling equation as commonly written, $x^* = A_x'' z^{*\prime\prime\beta}$, are y^* dependent; $\partial A_x''/\partial y^* = (A_x/A_y)(y/A_y)^{(1/\beta-1)}(1 - (y/A_y)^{(1/\beta)})^{(\beta-1)}$ and $\partial z^{*\prime\prime}/\partial y^* = (\partial/\partial y^*)((z^* - y^{*1/\beta}/A_y^{\,1/\beta})/(1 - y^{*1/\beta}/A_y^{\,1/\beta}))$. Were a sufficiently broad and detailed data net available, the analysis would permit the recovery of the derivatives $(\partial r^0{}_{hcp}^{-1}/\partial P)_{y_D,z_D}$, $(\partial r^0{}_{hcp}^{-1}/\partial y_D)_{z_D,P}$, $(\partial r^0{}_{hcp}^{-1}/\partial z_D)_{y_D,P}$, $(\partial T^0{}_{hcp}/\partial P)_{y_D,z_D}$, $(\partial T^0{}_{hcp}/\partial y_D)_{z_D,P}$, and $(\partial T^0{}_{hcp}/\partial z_D)_{y_D,P}$, and the width parameters $A_{MW}{}^0$, $B_{MW}{}^0$, $A_p{}^0$, $A_{y_D}{}^0$, and $A_{z_D}{}^0$, and their P, y_D, and z_D derivatives. The present data net is too limited for the general treatment. However there are sufficient data on the (T, y_D, p) surface to exemplify the approach. Least squares scaling analysis (one term fits, $\beta = 1/2$) for $(y_D, T, P)_{c,z_D=0,PSh=13.5}$ data yields $(\partial y_D{}^{0\prime\prime}/\partial P) = 0.066$ MPa^{-1} and $(\partial A_{y_D}{}''/\partial P) = 4.5 \times 10^{-3}$ MPa^{-1} for $0 \le P/\text{MPa} \le 5$. (A more general equation can be written which includes coupling terms, but the implications of this elaboration have not been explored.)

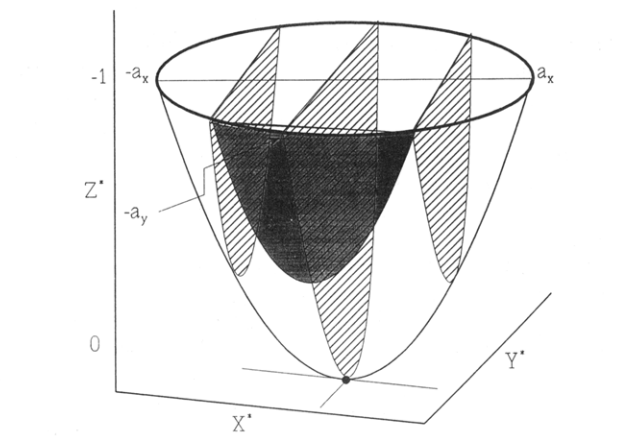

Figure 16. Three-dimensional ellipsoidal scaling surface (schematic, mean-field approximation). The origin of the surface is at the bottom and shown as the heavy dot, $(x^*, y^*, z^*) = (0, 0, 0)$. The equation for the 3D surface through the origin is $z^* = x^{*2}/A^2 + y^{*2}/B^2$. Two sections parallel to the z^* axis, whose planes intersect the master surface at $y = 0$ (not cross-hatched) and $y \approx -0.5$ (shaded) are shown. The equations for the lines of intersection of these planes with the master surface are $x^* = A(z^* - y^2/B^2)$. Similarly, three sections orthoganal to the first set (at $x^* = 0$ and $x^* \approx \pm 0.5$) are shown lightly cross-hatched. Relations between the (z^*, x^*) and (z^*, y^*) projections are developed in the text. The intersection of the $z^* = 1$ plane with the master surface defines an ellipse with major and minor axes equal to A and B, respectively.

7d. An Alternative Scaling Representation. We represent the excess free energy as $G^{ex} = \psi(1 - \psi)[g(\chi)]$ and apply a minor extension of the compelling description of phase equilibria given by Oonk.[48] A plot of $f(\chi) = [2\psi_c(1 - \psi_c)/R][g(\chi)_c - (1 - 2\psi_c)(\partial g(\chi)/\partial\psi)_c - (\psi_c(1 - \psi_c)/2)(\partial^2 g(\chi)/\partial\psi^2)]$ *vs* T has upper and lower critical points at the intersections with the diagonal. Positive curvature leads to an UCS/LCS conformation, negative curvature to a closed loop. The hypercritical point corresponds to the point where the diagonal first becomes tangent to $(T,f(\chi))$. It is convenient to transform coordinates from $(T,f(\chi))$, to the still orthogonal but 90° rotated system $(T',f(\chi'))$. Consider events when a change in a conjugate variable, η_k, is made along an axis orthogonal to the $(T',f(\chi'))$ plane. The perturbation, $\delta f(\chi') = \int(\partial f(\chi')/\partial\eta)\, d\eta$, can be expressed in terms of the free energy, $\delta G = 2^{1/2}\Delta f(\chi)$. To first order $\Delta G = -T\mathrm{d}S + V\mathrm{d}P + (\partial G/\partial\langle 1/r\rangle)\, \mathrm{d}\langle 1/r\rangle + (\partial G/\partial y_D)\, \mathrm{d}y_D + (\partial G/\partial z_D)\, \mathrm{d}z_D + \Sigma_i \mu_i \mathrm{d}\phi_i + \ldots$. Thus the entropy perturbation along the critical locus (not too far from T_{hcp}) scales as $\Delta T/T_{hcp}$, the pressure perturbation as $\Delta V/V$, the $\langle 1/r\rangle$ perturbation as $\Delta(\partial G/\partial\langle 1/r\rangle)/(\partial G/\partial\langle 1/r\rangle)$, *etc.* The choice of parameters η_k employed earlier now becomes obvious. For a given intensive variable, P, S, y_D, *etc.*, select its conjugate extensive variable at the hypercritical origin as reference. Thus a variation in S (not studied in this paper) should scale as $(\delta T/T_c)^{\gamma}$, one in P as $(\delta V/V_c)^{\gamma}$, *etc.* For example consider the pressure dependence, δ ln $V/\mathrm{d}P$, scales as $1/\kappa$ which sets the scaling parameter in eq 32 to $\Lambda_p \approx 1/\kappa_{solution}$ (approximated as $1/\kappa_{solvent}$ below). For $T_{hcp} \approx 360$ K, $\kappa_{acetone} \approx 2.5 \times 10^{-2}$ MPa^{-1} and $\Lambda_p \approx 40$ MPa.

7e. Comparison of Mean-Field and Scaling Fits. Experimental data of the quality and range presented

in this series of papers can be represented within experimental precision using either scaling or mean-field based equations. The advantage of the mean-field representation is that it allows one to fix some or all of the mean-field parameters independently of the phase-equilibrium measurements (*i.e.* using other thermodynamic data). Were excess volumes and excess enthalpy data available, eq 28 would permit a consistency check between the phase equilibrium data in the (T,P) plane and the excess property measurements. A second advantage of eq 28 is that it represents asymmetry in a straightforward fashion. Scaling representations require additional empirical terms. The present experiments do not establish either the scaling or the mean-field approach as "correct". Either approach is empirically useful. The data do not extend close enough to the hypercritical reference to test logarithmic scaling in a nonempirical fashion, or to establish the limiting exponent. That awaits more refined measurements very close to $(T,\eta)_{hcp}$. In the absence of excess enthalpy and excess volume data for these polymer solutions the mean-field representation is equally empirical.

8. Isotope Dependences y_D and z_D

The effect of D/H substitution on the phase diagrams is a focal point of the present work, this because in good approximation isotopic substitution does not change the potential energy surface describing the system. Szydlowski and Van Hook[1] have described a first order interpretation of the phase equilibrium isotope effect (PEIE) data which combines the principal features of symmetrical mixture theory[49] with the statistical theory of condensed phase isotope effects.[2-4] The present analysis offers an improved interpretation. It develops the excess free energy as a Redlich–Kister series, $G^{ex} = \psi(1 - \psi)[\chi_0 + \chi_1 (1 - 2\psi) + ...]$, but to sufficient precision the isotope and pressure dependences can each be described with one term. Thus the isotope effects are

$$\Delta G^{ex} = \psi(1 - \psi)[\chi_{0,1;y_D}(y_D - y_D^*) + \chi_{0,1;z_D}(z_D - z_D^*)] \quad (38a)$$

$$\Delta\mu_B^{ex} = (1 - \psi)^2[\chi_{0,1;y_D}(y_D - y_D^*) + \chi_{0,1;z_D}(z_D - z_D^*)] \quad (38b)$$

$$\Delta\mu_A^{ex} = \psi^2[\chi_{0,1;y_D}(y_D - y_D^*) + \chi_{0,1;z_D}(z_D - z_D^*)] \quad (38c)$$

For transfer from the perprotio reference ($y_D^* = z_D^* = 0$) to the perdeuterio solvent state ($y_D^* = 1$; $z_D^* = 0$), $\delta\Delta G^{ex}(A) = \psi(1 - \psi)[\chi_{0,1;y_D}]$, $\delta\Delta\mu_B^{ex}(A) = (1 - \psi)^2[\chi_{0,1;y_D}]$, and $\delta\Delta\mu_A^{ex}(A) = \psi^2[\chi_{0,1;y_D}]$, while the transfer free energies to the perdeuterio solute state are $\delta\Delta G^{ex}(B) = \psi(1 - \psi)[\chi_{0,1;z_D}]$, $\delta\Delta\mu_B^{ex}(B) = (1 - \psi)^2[\chi_{0,1;z_D}]$, and $\delta\Delta\mu_A^{ex}(B) = \psi^2[\chi_{0,1;z_D}]$.

The connection between the transfer free energy isotope effects and molecular properties is commonly discussed in terms of the Bigeleisen AB equation,[2-4]

$$\delta\Delta\mu_0^{\infty}/RT = A/T^2 + B/T \quad (39a)$$

$$A = (1/24)(hc/k)^2 \sum_i [(v_i'^2 - v_i^2)^{\infty} - (v_i'^2 - v_i^2)^0] \quad (39b)$$

$$B = (1/2)(hc/k) \sum_j [(v_j' - v_j)^{\infty} - (v_j' - v_j)^0] \quad (39c)$$

Here h is Planck's constant, c the velocity of light, and k the Boltzmann constant. The v's are vibrational frequencies (wavenumbers) and the prime designates the lighter isotope. The equation applies where the isotope sensitive vibrations of the molecules of interest (AC, MCP, or PS in the present case) fall neatly into two classes, a high-frequency set (indexed over j) which can be treated in the zero point energy (ZPE) approximation (the B term), and a low-frequency set (indexed over i), which includes the external vibrations and librations and the internal rotations, and which is to be treated in the high-temperature approximation (the A term). Also $(i_{max} + j_{max}) = 3n$; n is the number of atoms in the molecule under consideration.

We follow Szydlowski and Van Hook[1] and suggest the major portion of the isotope effect is accounted for with the ZPE (B) term associated with the carbon–hydrogen (carbon–deuterium) stretching modes as the molecule of interest is transferred from its pure reference state to infinite dilution in the other component. The free energies of transfer are available from the $\chi_{0,0;y_D}$ and $\chi_{0,0;z_D}$ parameters reported in Table 12. For acetone-*h vs* acetone-*d*/PS solutions the observed isotope effect, $\delta\Delta\mu_0^{\infty}$, is equivalent to a 9 cm^{-1} blue shift in each of the six carbon–hydrogen vibrations, for MCPh/PS// MCPd/PS the result in Table 12 corresponds to a $\approx$2 cm^{-1} blue shift in each of the eight stretches. The shifts in question refer to the transfer from the pure solvent reference to infinite dilution in the polymer. Typical ZPE shifts for transfer of van der Waals bonded fluids from the dilute gas to the liquid state are on the order of 8–12 cm^{-1} to the red, so the magnitude and sign of the calculated shifts are reasonable. In the region of the extrema in the phase diagrams where the experimental effort has been concentrated ($\psi \approx 0.15$), $\Delta\mu_A^{ex} \approx 0.15^2\chi_{0,1;y_D}$, which if expressed as an effective shift is much smaller. Although each polymer segment interacts with a large number of solvent vibrational modes (on the order of 6/0.15 $\approx$ 40 for AC, roughly the same for MCP solutions), the interaction with each individual mode is on a modest scale ($\approx$9/40 = 0.2 cm^{-1} for AC/PS).

It is interesting to compare the solute and solvent transfer isotope effects. The acetone/PS data show an isotope effect for PS deuteration which is opposite in sign but of about the same magnitude as the one for acetone deuteration. It is equivalent to a $\approx$7 cm^{-1} red shift *per* PS oscillator on the transfer of PS from the pure polymer reference to infinite dilution in solvent (AC). The equivalent figure for MCP solutions is $\approx$(1/2) cm^{-1}. Both the solute and the solvent shifts for the MCP solutions are markedly smaller than the corresponding shifts in AC solutions. The observation is compatible with chemical intuition. Finally, we note that it is remarkable that the rather complicated dependence of CP and SHDW on isotopic substitution, as exemplified, say, by Figures 8, 9, and 13, can be described nearly within experimental precision by a single free energy parameter (or, equivalently, a single frequency shift parameter) describing the solvent IE's, and another for the solute effects. Furthermore the parameters so deduced are consistent with those required to rationalize thermodynamic IE's in small molecule systems.

9. Conclusion

Experimental CP and SP demixing data have been obtained for polystyrene/solvent solutions and have been interpreted using a new approach. The dependences on

segment number, isotope (H/D) substitution, temperature, and pressure have been rationalized. The mean-field Flory–Huggins type analysis took polydispersity into explicit account *via* continuous thermodynamic analysis. Calculated cloud and shadow curves were compared with the experimental measurements. Along the critical line nonclassical scaling and mean-field expressions which usefully correlate the demixing data have been developed. The isotope effects on the phase equilibria, which are large, have been discussed by combining continuous thermodynamic Flory–Huggins analysis and condensed phase isotope effect theory. The net solvent and/or polymer zero-point-energy shifts required to rationalize the data are reasonable in sign and magnitude as judged both by isotope effect studies in small molecule systems and spectroscopic information.

Acknowledgment. This work was supported by the U.S. Department of Energy, Division of Materials Sciences. L.P.R. thanks the FLAD and JNICT-STRDA/C/CTM/626/92 foundations in Portugal for their support.

Supplementary Material Available: This supplementary material consists of Tables 2–5 (9 pages). Table 2 reports CP and SP data for liquid–liquid demixing in 65 acetone/polystyrene solutions as functions of temperature, pressure, concentration, molecular weight, and H/D substitution on solvent or solute. Table 3 reports least squares representations of CP and SP loci. Tables 4 and 5 similarly report data on 15 methylcyclopentane/polystyrene solutions. Ordering information is given on any current masthead page.

References and Notes

(1) Szydlowski, J.; Van Hook, W. A. *Macromolecules* **1991**, *24*, 4883.
(2) Bigeleisen, J. *J. Chem. Phys.* **1961**, *34*, 1485.
(3) Jancso, G.; Van Hook, W. A. *Chem. Rev.* **1974**, *74*, 689.
(4) Jancso, G.; Rebelo, L. P.; Van Hook, W. A. *Chem. Rev.* **1993**, *93*, 2645.
(5) Flory, P. J. *J. Am. Chem. Soc.* **1965**, *87*, 1833.
(6) Patterson, D. J. *J. Polym. Sci.* **1968**, *16C*, 3379.
(7) Sanchez, I. C. *Macromolecules* **1991**, *24*, 908.
(8) Panayiotou, C. G. *Macromolecules* **1987**, *20*, 861.
(9) Bates, F. S.; Wignall, G. D. *Macromolecules* **1986**, *19*, 932.
(10) Bates, F. S.; Wilthuis, P. *J. Chem. Phys.* **1989**, *91*, 3258.
(11) Kedrowski, C.; Bates, F. S.; Wilthuis, P. *Macromolecules* **1993**, *26*, 3488.
(12) Singh, R. R.; Van Hook, W. A. *Macromolecules* **1987**, *20*, 1855.
(13) Szydlowski, J.; Van Hook, W. A. *J. Polym. Sci. B. Polym. Phys.* **1991**, *29*, 1437.
(14) Szydlowski, J.; Rebelo, L. P.; Van Hook, W. A. *Rev. Sci. Instrum.* **1992**, *63*, 1717.
(15) Rebelo, L. P.; Van Hook, W. A. *J. Polym. Sci. B. Polym. Phys.* **1993**, *31*, 895.
(16) Siow, K. S.; Delmas, G.; Patterson, D. *Macromolecules* **1972**, *5*, 29.
(17) Zeman, L.; Patterson, D. *J. Phys. Chem.* **1972**, *76*, 1214.
(18) Saeki, S.; Kuwahara, N.; Hamano, K.; Kenmochi, Y.; Yamaguchi, T. *Macromolecules* **1986**, *19*, 2353.
(19) Hosokawa, H.; Nakata, M.; Dobashi, T. *J. Chem. Phys.* **1993**, *98*, 10078.
(20) Ratzsch, M.; Kehlen, H. *Prog. Polym. Sci.* **1989**, *14*, 1.
(21) Horst, R.; Wolf, B. A. *Macromolecules* **1991**, *24*, 2236.
(22) Kiepen, F.; Borchard, W. *Macromolecules* **1988**, *21*, 1784.
(23) Debye, P. *J. Chem. Phys.* **1959**, *31*, 680.
(24) de Gennes, P. *Scaling Concepts in Polymer Physics*; Cornell University Press: Ithaca, NY, 1979; Chapter 4.
(25) Rollins, K.; Scrivens, J. H.; Taylor, M. J.; Major, H. *Rapid Commun. Mass Spectrom.* **1990**, *4*, 355.
(26) Yijun, Y. *University of Tennessee, Internal Report*, 1991.
(27) Olabisi, O.; Robeson, L. M.; Shaw, M. T. *Polymer-Polymer Miscibility*; Academic Press: New York, 1979.
(28) Koningsveld, R. *Pure Appl. Chem.* **1989**, *61*, 1051.
(29) Schultz, A. R.; Flory, P. J. *J. Am. Chem. Soc.* **1952**, *74*, 4760; **1953**, *75*, 3888.
(30) Nakata, M.; Kuwahara, N.; Kaneko, M. *J. Chem. Phys.* **1975**, *62*, 4278.
(31) Nakata, M.; Dobashi, T.; Kuwahara, N.; Kaneko, M.; Chu, B. *Phys. Rev. A.* **1978**, *18*, 2683.
(32) Dobashi, T.; Nakata, M.; Kaneko, M. *J. Chem. Phys.* **1980**, *72*, 6685; **1980**, *72*, 6692.
(33) Singh, R. R.; Van Hook, W. A. *J. Chem. Phys.* **1987**, *87*, 6097.
(34) Cowie, J. M. G.; McEwen, I. J. *Polymer* **1984**, *25*, 1107.
(35) Van Hook, W. A. *Fluid Phase Equilibria* **1985**, *22*, 55.
(36) Numerical implementation of this method has been coded in a QUICKBASIC' computer routine, PHASEEQ', copyrighted by M. Lusczyk and W. A. Van Hook.
(37) Qian, C.; Mumby, S. J.; Eichinger, B. E. *Macromolecules* **1991**, 24, 1655.
(38) Mumby, S. J.; Sher, P. *Macromolecules* **1994**, *27*, 689. Although a polydisperse formalism is developed in this reference, all calculations which compare results with experiment are made in the monodisperse approximation.
(39) Solc, K. *Macromolecules* **1970**, *3*, 665.
(40) Solc, K.; Kleintjens, L. A.; Koningsveld, R. *Macromolecules* **1984**, *17*, 573.
(41) Solc, K.; Koningsveld, R. *J. Phys. Chem.* **1985**, *89*, 2237.
(42) Kamide, K. *Thermodynamics of Polymer Solutions*; Elsevier: Amsterdam, 1990.
(43) Hu, Y.; Ying, H.; Wu, D. T.; Prausnitz, J. M. *Macromolecules* **1993**, *26*, 6817.
(44) Bawendi, M. G.; Freed, K. F. *J. Chem. Phys.* **1988**, *88*, 2741.
(45) Luszczyk, M. *J. Chem. Thermodynam.* **1988**, *20*, 29.
(46) Lusczyk, M.; Van Hook, W. A. *Macromolecules* to be submitted.
(47) Prausnitz, J. M. *Molecular Thermodynamics of Fluid-Phase Equilibria*; Prentice Hall: Englewood-Cliffs, NJ, 1969.
(48) Oonk, H. A. J. *Phase Theory*; Elsevier: Amsterdam, 1981.
(49) Guggenheim, E. A. *Application of Statistical Mechanics*; Clarendon Press: Oxford, U.K., 1966.

MA941150V